Temperate Oligocene surface ocean conditions offshore Cape Adare, Ross Sea, Antarctica

Frida S. Hoem[1], Luis Valero[2], Dimitris Evangelinos[3], Carlota Escutia[3], Bella Duncan[4], Robert M. McKay[4], Henk Brinkhuis[1,5], Francesca Sangiorgi[1], and Peter K. Bijl[1]

[1]Department of Earth Sciences, Utrecht University, Utrecht, The Netherlands, [2]Department of Earth Sciences, University of Geneva, Geneva, Switzerland, [3]Instituto Andaluz de Ciencias de la Tierra (CSIC-UGR), Armilla, Spain, [4]Antarctic Research Centre, Victoria University of Wellington, Wellington, New Zealand, [5]Royal Netherlands Institute for Sea Research (NIOZ), Texel, The Netherlands

Correspondence to: Frida S. Hoem (f.s.hoem@uu.nl)

Abstract. Antarctic continental ice masses fluctuated considerably during the Oligocene "coolhouse", at elevated atmospheric CO_2 concentrations of ~600–800 ppm. To assess the role of the ocean on the Oligocene ice sheet variability, reconstruction of past ocean conditions in the proximity of the Antarctic margin are needed. While relatively warm ocean conditions have been reconstructed for the Oligocene offshore Wilkes Land, the geographical extent of that warmth is unknown. In this study, we reconstruct past surface ocean conditions from glaciomarine sediments recovered from Deep Sea Drilling Project (DSDP) Site 274, offshore the Ross Sea continental margin. This site, located offshore Cape Adare is ideally situated to characterise Oligocene regional surface ocean conditions, as it is situated between the colder, higher-latitude Ross Sea continental shelf, and the warm-temperate Wilkes Land Margin in the Oligocene. We first improve the age model of DSDP Site 274 using integrated bio- and magnetostratigraphy. Subsequently, we analyse organic walled dinoflagellate cyst assemblages and lipid biomarkers (TEX_{86}) to reconstruct surface paleoceanographic conditions during the Oligocene (33.7–24.4 Ma). Both TEX_{86}-based sea surface temperature (SST) and microplankton results show temperate (10–17°C ± 5.2°C) surface ocean conditions at Site 274 throughout the Oligocene. Oceanographic conditions between offshore Wilkes Land margin and Cape Adare became increasingly similar towards the late Oligocene (26.5–24.4 Ma), inferred to be the consequence of the widening of the Tasmanian Gateway, which resulted in more interconnected ocean basins and frontal systems. To maintain marine terminations of terrestrial ice sheets in a proto-Ross Sea with as warm offshore SSTs as our data suggests, requires a strong ice flux fed by intensive precipitation in the Antarctic hinterland during colder orbital states, but with extensive surface melt of terrestrial ice during warmer orbital states.

1. Introduction

The Southern Ocean plays a crucial role in global ocean circulation, stability of the Antarctic ice sheet and the carbon cycle. At present, strong temperature gradients isolate Antarctica from the influence of warmer surface water from lower latitude regions. Despite its crucial role, still little is known about the evolution of Southern Ocean. Southern Ocean surface conditions cooled during the mid Eocene (<49 Ma; Bijl et al., 2009; 2013), which culminated with the initiation of Antarctic continental-scale glaciation at the Eocene-Oligocene transition (EOT~33.7 Ma; Zachos et al., 1994; Coxall et al., 2005; Bohaty et al., 2012). The overall higher bedrock elevation

and larger subaerial area of Antarctica during the Oligocene (33.9–23.0 Ma; Gradstein et al., 2012) (Wilson et al., 2013; Paxman et al., 2019) allowed for the occupation of large terrestrial ice caps. Antarctic ice-proximal records suggest that these ice sheets extended onto the coast, forming ice margins with marine terminations (Escutia et al., 2011; Scher et al., 2011; Galeotti et al., 2016). Apparently, Southern Ocean temperatures at the earliest Oligocene oxygen isotope step (EOIS) cooled sufficiently to sustain the marine-terminating ice sheets. Following the EOIS, gradually deep-sea $\delta^{18}O$ rebounded (Zachos et al., 2008), suggesting long-term loss of Antarctic ice, and/or gradual deep-sea warming. Indeed, the Oligocene remained a relatively warm time interval globally (O'Brien et al., 2020). However, on orbital time scales, Oligocene Antarctic ice volume underwent major fluctuations in size (e.g., Pälike et al., 2006; Galleoti et al, 2016; McKay et al., 2016; Liebrand et al., 2017; Levy et al., 2019), and as of yet the role Southern Ocean sea surface temperature (SST) conditions played in these fluctuations remains poorly understood, mostly because of a sparse geographic coverage of reconstructions of Oligocene SSTs.

Warm-temperate Oligocene SSTs (13–25°C) and frontal system reconstructions at the Wilkes Land margin were derived from organic walled dinoflagellate cyst (dinocyst) assemblages at Deep Sea Drilling Project (DSDP) Site 269 (Evangelinos et al., 2020) and Integrated Ocean Drilling Program (IODP) Site U1356 (Bijl et al., 2018b). These were corroborated with quantitative SSTs based on organic biomarkers (TEX_{86}; Hartman et al., 2018), and sedimentological and lithological interpretations (Salabarnada et al., 2018; Evangelinos et al., 2020). Data seem to indicate a southward displacement of the (proto-) Southern Ocean fronts, perhaps favoured by the still constricted, narrow Tasmanian Gateway (Scher et al., 2015), and consequent southward deflection of warm ocean currents (Fig. 1b). The relative absence of iceberg-rafted debris in most of the Oligocene sedimentary record of IODP Site U1356 (Escutia et al., 2011; Salabarnada et al., 2018; Passchier et al., 2019) suggests that the East Antarctic Ice Sheet (EAIS) at the Wilkes Land sector may have been predominately land-based, indicating limited ice sheet-ocean interaction in this sector of the EAIS. Sedimentary records recovered from cores located near the Transantarctic Mountain outlet glaciers, such as DSDP Site 270 (Kulhanek et al., 2019), CIROS-1 (Barrett et al., 1989) and Cape Roberts Project (CRP) (Naish et al, 2001; Prebble et al., 2006; Houben et al., 2013) have provided important insights into widespread advances of both East and West Antarctic Ice Sheet terminating into the western Ross Sea. TEX_{86}-based SST records indicate lower temperatures (6–14°C) in the Ross Sea during the Oligocene (Levy et al., 2016; Duncan, 2017) than offshore the Wilkes Land margin (Hartman et al., 2018), suggesting a large (~ 7°C), much larger than present, (sub-)surface ocean temperature difference between the two sectors. However, it remains unknown whether the warm conditions offshore the Wilkes Land margin were unique or whether similar temperatures existed close to the Ross Sea continental shelf in the Oligocene.

To this end, we investigated sediments recovered during DSDP Leg 28 at Site 274, located on the continental rise offshore the Ross Sea, ~ 250 km northwest of Cape Adare (Hayes et al., 1975), which is at an intermediate location between the aforementioned sites in the Ross Sea and offshore Wilkes Land (Fig. 1). DSDP Leg 28 retrieved valuable sedimentary records from the continental shelf and rise regions of the Ross Sea, but poor age control has long hampered their use in reconstructing past ocean conditions. Moreover, the archives were devoid of calcareous foraminifers, denying the use of their wall-geochemistry, typically used for the reconstruction of ocean conditions. Studies based on dinocysts have however allowed both age control and paleoceanographic interpretations, as e.g.,

a result of the established connection between dinocyst assemblage composition and surface water conditions of present-day Southern Ocean (Prebble et al., 2013; Zonneveld et al., 2013; Marret et al., 2019). Recent dinocyst records from the Ross Sea region (notably CRP (Clowes et al., 2016) and DSDP Site 270 (Kulhanek et al., 2019)), and from Wilkes Land (IODP Site U1356 (Sangiorgi et al., 2018; Bijl et al., 2018a, b) and DSDP Site 269 (Evangelinos et al., 2020)) provided new biostratigraphic constraints. We used these constraints, alongside new biostratigraphic and magnetostratigraphic analyses to improve the age model of DSDP Site 274. We then interpret paleoceanographic conditions with dinocyst assemblages, and generate quantitative SST reconstructions with lipid biomarkers (TEX_{86}). By comparing these results with available reconstructions from the Ross Sea and Wilkes Land in selected time slices, we evaluate how surface oceanographic conditions changed and latitudinal heat transport developed through the Oligocene.

2. Material

2.1 Site description

DSDP Site 274 (68°59.81'S; 173°25.64'E; 3326 m water depth, Fig. 1a), is located on the lower continental rise in the northwestern Ross Sea, about 250 km north-northeast of Cape Adare (Hayes, 1975). Sediments were collected using punch core-rotary drilling on the *Glomar Challenger* in February 1973 (Hayes, 1975). Currently, the region is seasonally covered by sea ice (Fetterer et al., 2020) and present-day mean annual SST is ~ -1°C (Locarnini et al., 2019). The site is in the vicinity of the southern upwelling margin of the Antarctic Divergence and currently located in the path of a major outflow for Antarctic Bottom Water, spilling out over the western Ross Sea continental shelf where it is deflected westward (Orsi and Wiederwohl, 2009). The location of DSDP Site 274 is ideal for studying the Oligocene oceanic properties offshore the Ross Sea (Fig. 1b), which we compare to documented Antarctic ice sheet and ocean conditions from proximal Ross Sea records (Fig. 1a).

2.2 Lithology and depositional settings

Drilling at DSDP Site 274 penetrated 421 meters below the sea floor (mbsf) and recovered a total of 43 cores containing 275.5 meters of sediment. We focus our study on the interval between 174.2 and 408.5 mbsf (Cores 19-43)(Fig. 2a). Sediment within this interval is mainly composed of (i) diatom-rich detrital silty clay with varying abundances of diatoms, from trace amounts to up to 80% (diatom ooze) (174.2–328 mbsf); and (ii) silty claystones and interbedded chert layers (328–408.5 mbsf). Scattered iceberg-rafted debris (IRD; pebbles, granules) have been documented between 152 and 323 mbsf. Below 323 mbsf, chert layers compromised core recovery and at 415 mbsf the basalt basement was reached (Hayes et al., 1975). The sediment cores are rather homogenous and lack strong sedimentary structures. The strong biscuiting and fracturing of lithified sediment testifies to drilling disturbance due to the rough nature of rotary drilling, and may have obscured depositional sedimentary structures. Downslope transport of sediment from the Ross Sea continental shelf to the site potentially complicates the reconstruction of local pelagic-derived ocean conditions. The lithology and the seismic patterns (Hayes et al., 1975) suggest that sediment in the Oligocene was transported and deposited within the Adare Basin through a combination of downslope gravity currents and subsequent reworking by bottom currents (Hayes et al., 1975).

3. Methods

3.1 Age model

The shipboard age model (Hayes et al., 1975), based on few biostratigraphic (diatom, radiolarian and calcareous nannofossils) age tie points, initially dated the DSDP Site 274 sedimentary record overlying the basalt to late Eocene – Quaternary. More recently, Cande et al. (2000) dated the ocean crust underneath DSDP Site 274, using paleomagnetic data, to chron 13, ∼33.5 Ma, which is 200 kyr younger than the EOT, and 5-7 Myrs younger than dated during the expedition (Hayes et al., 1975). Granot et al. (2010) formulated seismic stratigraphic units, and correlated these units onto the Ross Sea continental shelf. The lowermost regional unconformity (328 mbsf) above the basement (Hayes et al., 1975) corresponds to a Ross Sea unconformity (RSU) found in the Northern Basin, RSU6, estimated to be of early Oligocene age (34–26.5 Ma; De Santis et al., 1995; Granot et al., 2010; Kulhanek et al., 2019). The major unconformity at 180.5 mbsf, between Cores 19 and 20 (Hayes et al., 1975) is tied to seismic reflectors RSU4 and RSU4a (Granot et al., 2010), aged middle Miocene, ∼15.8–14.6 Ma and ∼17/16.9 Ma respectively (Pérez et al., 2021). To further improve the age model, we generated new age tie points based on dinocyst biostratigraphy and magnetostratigraphy to better constrain the age of the sedimentary record (Core 43–17). Dinocyst biostratigraphy follows Bijl et al. (2018a) who reassessed dinocyst species first and last occurrence datums calibrated against the international geological time scale GTS 2012 (Gradstein et al., 2012). Magnetic reversals on the sediment samples were identified through stepwise demagnetization experiments performed using the 2G magnetometer with an inline alternating fields (AF) demagnetiser attached to an automatic sample handler in Fort Hoofddijk (Utrecht University), and the 2G-SRM750 Superconducting Rock Magnetometer housed at the Paleomagnetic Laboratory of Barcelona (CCiTUB-CSIC). As core orientation is not reconstructed, magnetic declinations are discarded and only magnetic inclinations are used to determine polarities. Recently, Jovane et al., (2020) carried out a paleomagnetic study at the DSDP Site 274, focusing on magnetic properties and magnetic mineralogy characterization, and by means of a review of the available biostratigraphic constraints they also propose a new age model. Here, we compare their age model with ours and we discuss the differences.

3.2 Organic geochemistry

To reconstruct sea (sub-) surface temperature (SST) we applied the TEX_{86} (TetraEther indeX of 86 carbon atoms) proxy (Schouten et al., 2002), based on the temperature-dependent cyclization of isoprenoidal glycerol dialkyl glycerol tetraethers (GDGTs) produced by thaumarchaeotal membrane lipids. GDGTs were extracted from powdered and freeze-dried sediments using an accelerated solvent extractor. Lipid extracts were then separated into an apolar, ketone and polar fraction by Al_2O_3 column chromatography using hexane:DCM (9:1, v:v), hexane:DCM (1:1) and DCM:MeOH (1:1) as respective eluents. Of a synthetic C_{46} (mass-to-charge ratio, m/z = 744) 99 ng GDGT standard was added to the polar fraction, which subsequently was dissolved in hexane:isopropanol (99:1, v/v) to a concentration of ~3 mg ml^{-1} and filtered over a 0.45-µm polytetrafluoroethylene filter. The dissolved polar fractions were injected and analysed by high-performance liquid chromatography–mass spectrometry (HPLC–MS), using double-column separation (Hopmans et al., 2016). GDGT peaks in the HPLC chromatograms were integrated using ChemStation software.

3.2.1. TEX_{86} calibrations

Several calibrations exist to convert TEX_{86} values into SSTs based on modern core–top datasets (Kim et al., 2010). We follow the discussion by Hartman et al. (2018), and used the linear calibration by Kim et al. (2010) to calculate the TEX_{86}-SST relations which include the high-latitude core-top values. As we present peak areas of individual GDGTs in the supplements (Table S2), other calibrations can be plotted as well.

3.2.2 TEX_{86} overprints and bias

We use ratios of GDGTs as proxies to detect potential overprinting factors that may bias the pelagic signature of the sedimentary GDGTs. The relative contribution of terrestrial GDGT input has been reconstructed using the branched and isoprenoid tetraether (BIT) index (Hopmans et al., 2004). Samples with BIT index values >0.4 may be biased by soil- and river-derived GDGTs (Bijl et al., 2013). However, we do note that the validity of this proxy for soil organic matter input is questioned, now that it becomes clear that branched GDGTs may also be produced in the marine realm (Peterse et al., 2009; Sinninghe Damsté, 2016), and terrestrial ecosystems that also contain crenarchaeol (Pearson et al., 2004). The methane index (Zhang et al., 2011) flags overprint by sedimentary methanogenic activity, GDGT-2/GDGT-3 ratio (Taylor et al., 2013) signals overprint by archaeal communities dwelling deeper into the water column and GDGT-0/Crenarchaeol ratio (Blaga et al., 2009; Sinninghe Damsté et al., 2009; Taylor et al., 2013) flags overprint by in situ production of isoprenoidal GDGTs in lakes and rivers, and contribution from Euryarchaeota. The ring index (Zhang et al., 2016), can detect deviations from a pelagic character in the GDGT 'assemblage'. Samples which had overprinting values in these biasing indices were marked as unreliable. High-latitude TEX_{86}-SST reconstructions are believed to be skewed towards summer temperatures (Schouten et al., 2013; Ho et al., 2014), but studies around Antarctica, have found archaea appear most abundantly in winter and early spring, with maximum abundances in the subsurface at around 100 m (e.g., Church et al., 2003; Kalanetra et al. 2009; Massana et al. 2009). However, there is a general agreement that TEX_{86} captures the relative SST trend (Richey and Tierney, 2016) remarkably well despite these uncertainties, and this will be our main focus when interpreting the results.

3.3 Palynology

3.3.1 Palynological processing and taxonomy

A total of 50 samples, 2 per core (Core 43–17), were processed for palynology by using palynological processing and analytical procedures of the Laboratory of Palaeobotany and Palynology, published previously (e.g., Bijl et al., 2018a). Freeze-dried or oven-dried sediment was crushed and weighed (on average 10 g, SD: <1 g). A tablet of a known amount of *Lycopodium clavatum* spores (a marker grain) was added prior to palynological processing to allow for quantification of the absolute number of dinocysts per sample. In order to digest carbonates and silicates, the sediment was treated with 30% HCl overnight first to remove calcium carbonate, 38% HF overnight to digest silicates, 30% HCl was then added to remove fluoride gels, and subsequently centrifuged and decanted. Organic residues were isolated between 250 µm and 10 µm sieve meshes, with the help of an ultrasonic bath to break down and clear out agglutinated organic particles. Residues were mounted on glass slides using glycerine jelly. Palynomorphs were counted using a Leica DM2500 LED transmitted light optical microscope. While the main focus was on dinocysts, terrestrial palynomorphs, acritarchs and prasinophyte algae (unicellular planktonic

autotrophs) were quantified as well, and the presence and relative abundance of other organic remains were noted. Dinocyst taxonomy follows Williams et al. (2017), Clowes et al. (2016) and informal species as presented in Bijl et al. (2018a). Specimens were identified to a species level when possible. A minimum of 200 identifiable dinocysts were counted per slide at 400x magnification, while the remainder of the slide was scanned at 200x magnification to identify rare taxa not observed during the regular count. Samples with counts of <50 in situ specimens were discarded for qualitative assessment. All slides are logged in the collection of the Laboratory of Palaeobotany and Palynology, Utrecht University.

3.3.2 Dinocyst paleoecological affinity

Present-day surface sediment distribution of dinocysts depends mostly on surface water temperature, but also on nutrient availability, salinity, primary productivity and sea-ice cover (Dale, 1996; Prebble et al., 2013; Zonneveld et al., 2013). We assume that habitat affinities and trophic levels of modern dinoflagellate species remained similar throughout the Oligocene and Neogene, although for a very limited number of species (e.g., *Impagidinium pallidum*) shifts in environmental preferences have been demonstrated (de Schepper et al., 2011). Here we use the modern relationship between dinocyst occurrence and properties of the overlying water to infer oceanographic conditions in the past for extant species (Bijl et al., 2013; Prebble et al., 2013). To determine the habitat affinities and trophic level of extinct dinoflagellates, we rely on previously published papers where a link to paleoceanographic proxies for temperature, runoff/fresh water input, and nutrient conditions was demonstrated (Bijl et al., 2011; 2018a; Frieling and Sluijs, 2018; Egger et al., 2018). We separate the dinocyst assemblages into Gonyaulacoid (G) and Protoperidinioid (P) cysts. In the Southern Ocean, G-cyst generally include phototrophic temperate dinocysts, associated with warm oligotrophic, open water conditions (Prebble et al., 2013). At present, G-cysts are rare in close proximity of the Antarctic ice sheet (Prebble et al., 2013). An exception is *Impagidinium pallidum* which today is found in low percentages in Antarctic environments in the vicinity of the polar front (Zonneveld et al., 2013). The extant *Operculodinium* spp., *Pyxidinopsis* spp. *Corrudinium* spp., *Impagidinium* spp. and *Nematosphaeropsis labyrinthus* are absent or represent a minor component of the polar assemblages. P-cysts are produced by heterotrophic dinoflagellates and are usually found in nutrient-rich environments: river outlets, upwelling areas, and sea-ice zones (Zonneveld et al., 2013).. In the Southern Ocean today, where the Antarctic Divergence upwelling favours a dominance of P-cysts, species such as *Brigantedinium* spp., *Selenopemphix* spp., especially *S. antarctica*, are common (Prebble et al., 2013). *S. antarctica* is a species that shows affinity to sea-ice conditions (Zonneveld et al., 2013; Marret et al., 2019).

3.3.3 Reworked versus in situ dinocysts

One issue of studying sediment records in the proximity of glaciated margins is separating reworked from in situ species, which is needed for obtaining reliable biostratigraphic constraints and paleoceanographic signals (Macphail, 2021). In turn, quantifying the history of reworked material through time may yield information about the depositional conditions on the Ross ice shelf. In this study, we follow the interpretations of Bijl et al. (2018a) and a priori separated dinocyst species into an assumed reworked and an in situ group (Table 1). We applied statistical analysis to test a priori assumptions (Bijl et al., 2018a) on in situ or reworked dinocyst species and to quantitatively measure co-variability between environmental variables and palynological data. Our palynological data were analysed using Correspondence analysis (CA), a linear ordination method to explore the differences in

assemblages between samples. The palynological data (relative abundance) were plotted in the C2 software program (Juggins, 2007) using square root transformation.

4. Results

4.1 Revised age model

Based on four new dinocyst-based first occurrence (FO) and last occurrence (LO) datums found in the DSDP Site 274 record we provide additional age constraints to the age model upon which we correlate five new paleomagnetic reversal results to specific magnetic chrons (based on Gradstein et al., 2012; Table 2). Paleomagnetic results are generally of low quality (Fig. 2b). We interpret this to result from both a low natural remnant magnetization (NRM) intensity (typically between 10–50 A/m^2) and the likely growth of iron sulfides during ~50 years storage of the cores, which probably are the cause of magnetic noise as well as the partial isolation of the characteristic component in some samples (Fig. S1; Table S1). Because the low quality of results, we are cautious and only confident in those magnetozones with at least 3 adjacent samples sharing similar polarity values. Cores 23 to 19 express a well-defined polarity pattern. Below, the interval encompassing cores 26 to 28 (269.12–214.43 mbsf, in grey Fig. 2b) does not show a definite pattern and consequently was not considered for paleomagnetic correlation. The lower part, cores 35 to 43, has a very low recovery and is prone to normal polarity directions. Magnetostratigraphic results for the upper Oligocene generally agree with those recently published by Jovane et al. (2020; Fig. 2). For the lower part of the record, our biostratigraphic results provide new tie-points that indicate lower Oligocene age, instead of the previously published upper Eocene age (Hayes et al., 1975; Jovane et al., 2020).

The presence of marker dinocyst *Malvinia escutiana* (FO = 33.7 Ma; Houben et al., 2011; Houben et al., 2019) in the lowermost sediment sample (Core 43, 404.66 mbsf) directly overlying the basement, indicates an Early Oligocene age of the lowermost sediment that was also suggested from the age of the underlying ocean crust (Cande et al., 2000). Thus, we correlated the normal magnetozone in Core 43 (400.7 mbsf) with magnetic chron C13n. A few sections above we find the FO of *Stoveracysta ornata* (32.5 Ma) at 396.62 mbsf. The FO of *Operculodinium eirikianum* (31.56 Ma) 352.78 mbsf, the FO of *Corrudinium labradori* (30.92 Ma) at 362.42 mbsf and the LO of *Stoveracysta ornata* (30.8 Ma) is found at 323.6 mbsf. Thus we suggest, the reversal at the lower part of Core 34 (321.2 mbsf) to correlate with the top of C11n.1n (29.18 Ma) and the normal magnetozone found in Cores 29 and 30 (277 mbsf), to correlate with chron C9n (Table 2). Core 21 (∼190.8 mbsf) contain one isolated calcareous nannofossil horizon (Burns, 1975) dominated by *Chiasmolithus altus*, which marks an oldest age of 25.44 Ma (Chron C8n, Gradstein et al., 2012). Cores 34–20 are included in the diatom *Pyxilla Prolungata* zone (Hayes et al., 1975), which also suggests an early Oligocene age (>25 Ma), however the last occurrence of *Pyxilla Prolungata* is discussed to go on until Oligocene – Miocene boundary (23 Ma) (Gombos et al., 1977). Based on these initial report biostratigraphic observations (Hayes et al., 1975), we here correlate the base of normal magnetozone of Core 21 (199.47 mbsf) with the base of chron C7n.2n (24.4 Ma). A few biostratigraphic constraints, including middle Miocene radiolara species in Core 19 (Hayes et al., 1975) indicate that the latest Oligocene and Oligocene – Miocene transition is missing in a large hiatus of ~7 Myr between Cores 19 and 20 (181.23 mbsf). We abstain from correlating the normal magnetozone of Core 19 to a specific chron, due to the

limited biostratigraphic markers, and thus we here support Jovane et al., (2020), who suggested Langhian to Burdgalian ages. Extrapolating linearly between chrono- and biostratigraphic tie points (Fig. 2b; Table 2) we calculate the average sedimentation rate in the Oligocene to be 2.4 cm/kyr.

4.2 Lipid biomarkers

Thirty-nine of the 42 samples processed for lipid biomarkers showed no indication of overprints by biasing indices (Fig. S2). The low BIT index value (<0.08, with one exception at 361 mbsf; Fig. S2) suggests low terrestrial organic material influence, relative to marine GDGT production. The normal Ring index values (Fig. S3), with only two outliers, suggests normal pelagic contributions to the sedimentary GDGTs. Thus overall, TEX_{86} values represent an in situ pelagic SST signal. Moreover, the absence of co-variance between TEX_{86} and indices for overprint suggest the high variability in TEX_{86} also represents a pelagic signal. TEX_{86} values range from 0.44 to 0.55. Using the linear calibration of Kim et al. (2010) (Fig. 4c), SSTs vary between 10–17°C (±5.2°C) throughout the record, with noticeable variability. Below 342 mbsf, reconstructed SSTs are relatively high, and variable (10–16°C). Between 335–248 mbsf SSTs are lower and display lower variability (10–13°C) at the same sample resolution as above. An increase in SST of ~6°C at 248 mbsf marks the onset of a second interval with high variability in SST.

4.3 Palynomorphs and dinocyst assemblages

Forty-three of the 50 samples analysed contain sufficient dinocysts. All samples that were too low in dinocysts came from the top of the studied record (186.66–155.68 mbsf), and were discarded. Samples showed varying abundance of four palynomorph groups: reworked dinocysts, in situ dinocysts, terrestrial palynomorphs and acritarchs and prasinophytes (Fig. 4a). The sediments below 352.5 mbsf are dominated by reworked dinocysts, which decrease in abundance above this depth. From 352.5 mbsf to the top of the record, in situ dinocysts constitute the most abundant palynomorph group, followed by acritarchs, which slightly increase upcore. Pollen and spores remain low throughout the entire record (<6%). Furthermore, our palynological samples contain a varying amount of pyritized microfossils and amorphous organic material.

4.3.1 Dinocyst taxonomy

Identification of dinocysts on a species level was possible in most cases (Table S3). However, some dinocysts were only defined on a genus level when distinctive features were lacking. *Brigantedinium* spp. includes all round-brown specimens. *Batiacasphaera* spp. includes small, sub- spherical cysts with an angular, likely apical archeopyle, and if any, minute surface ornamentation. *Pyxidinopsis* spp. have similar features to *Batiacasphaera* spp. but is typcially (even) smaller, has a thicker, slightly darker wall, and is less folded with a single plate precingular archeopyle. Dinocysts with a smooth, spherical, psilate, hyaline wall and a free, angular- rounded operculum, 5–6 sides, generally found within the cyst are hereby informally named Dinocyst sp. 1. The saphopylic archeopyle of Dinocyst sp.1, resembles that of *Brigantedinium* spp. and *Protoperidinium* spp. and for this reason we consider Dinocyst sp. 1 as belonging to the (heterotrophic) Protoperidinioid (P) cysts.

4.3.2 Reworked dinocyst assemblages

The lowermost 60 m of the sediment record, below 352.5 mbsf, yield abundant and diverse dinocysts, that are common in Eocene Southern Ocean sediments (Bijl et al., 2013; Cramwinckel et al., 2020; Crouch et al., 2020) including *Vozzhennikovia apertura, Deflandrea antarctica, Enneadocysta* spp. and *Phthanoperidinium* spp. These species are found throughout the entire record, but their relative abundance decreases upsection. We note good preservation of some of the more delicate dinocysts, which have known biostratigraphic ranges that predate the age of the ocean crust underneath DSDP Site 274, therefore we still regard them to be reworked. However, we cannot rule out that these typical late Eocene dinocysts were still present in the early Oligocene and therefore in situ deposited in the record (Bijl et al., 2018a).

4.3.3 In situ dinocyst assemblages

In the lowermost 15 m of the record, below 390.4 mbsf, the (apparent) in situ assemblage (Fig. 4b) is dominated by P-cyst species Dinocyst sp.1 and *Brigantedinium* spp., indicating high nutrient levels in open ocean settings. Given that *Brigantedinium* spp. has preference for open ocean conditions, often with proximity to upwelling areas both in the modern and the ancient ocean (Zonneveld et al., 2013; Sluijs et al., 2005), we render it unlikely that it was transported from the continental shelf and reworked. *Brigantedinium* spp. and Dinocyst sp. 1 have not been reported from CRP-3 (Clowes et al., 2016) or the Eocene erratics (Levy and Harwood, 2000) from the Ross Sea area. The good preservation state of the delicate species Dinocyst sp.1 and *Brigantedinium* spp., argues for in situ production. The extinct P-cyst species *Malvinia escutiana* occurs throughout the record: its relative abundance increases from the bottom of the record towards its peak interval from 224 mbsf to the top of the record. At about 335 mbsf, the dinocyst assemblages change significantly. Above this depth, G-cysts associated with open, possibly warmer and oligotrophic waters dominate the assemblages. This shift in the dinocyst assemblage does not coincide with any remarkable change in the lithology. Hence, we are confident that the assemblage shift is a real feature in the record and not a result of the selective preservation of P and G cysts. It is known that P-cysts are more sensitive than G-cysts to oxidation (e.g., Zonneveld et al., 2010). and any mechanism (bottom currents, mixing, sediment starvation) which favours sediment oxygenation, would decrease the probability of finding P-cysts preserved in the record relatively to G-cysts. *Batiacasphaera* spp*., Pyxidinopsis* spp. and *Cerebrocysta* spp. compose the majority of the G-cysts. *Spiniferites* spp. is relatively abundant (~10–20% of the total in situ dinocyst counts) in the interbedded chert layers below 352.5 mbsf and again, but less prominent, at 221.4 mbsf, while it remains low (<4%) in the rest of the record. *Operculodinium* spp. is common (10–20%) between 201–221 mbsf. The highest amount of *Operculodinium* spp. (27%) was found at 239.16 mbsf. *Nematosphaeropsis labyrinthus* is only registered between 361–352 mbsf (green line Fig. 4b). *Impagidinium* spp. remain low (< 7%) in all samples. Throughout the record, cold water indicative dinocyst species are rare. *Selenopemphix antarctica*, a major component of the modern Antarctic-coastal assemblages (Zonneveld et al., 2013), is never abundant, and present only in few samples (between 390.44–333 mbsf, and at 302 mbsf). *I. pallidium*, a dinocyst abundant in polar areas of the modern ocean (Zonneveld et al., 2013; Marret et al., 2019), but known for its tolerance to higher temperatures in the past (de Schepper et al., 2011) has a scattered low presence throughout the record.

4.3.4 Other palynomorphs: Pollen, acritarchs and prasinophyte algae

The consistently sparse pollen assemblages from DSDP Site 274 suggest a shrubby tundra landscape with low-growing Nothofagaceae and Podocarpaceae. The offshore and off-path location to the wind patterns from the continent, may be an explanation for the low pollen numbers, and we cannot make further interpretations to the terrestrial ecology. The relative abundance of acritarchs and prasinophytes seems to increase upcore. Transparent chorate acritarchs is the most dominant throughout the record. *Leiosphaeridia* spp. is only sporadically present, and most common in the lowermost sediments (>390 mbsf). Prasinophyte algae *Cymatiosphaera* spp. is found throughout the record, but more abundantly around 285 mbsf, and above 224 mbsf.

4.4 Correspondence analysis

The CA on our palynological results (Fig. 3, Table S4) resulted in the first two axes explaining 46% of the total variance (31% for axis 1 and 15% for axis 2), which is high, given the multidimensionality of the high dinocyst diversity. Most of the dinocysts assumed reworked a priori (purple in Fig. 3) show negative scores on axis 2 (64%). Those taxa that do not have a negative score on axis 2, have generally low total counts or relative abundances (small circles in Fig. 3). Overall, the species we consider to be definitely in situ (see also Bijl et al., 2018a) have negative scores on axis 1, and reworked taxa tend to cluster on the positive side of axis 1. Terrestrial palynomorphs (pollen and spores) plot in the same area as the reworked dinocyst taxa. The overall separation of reworked and in situ taxa on the first CA axis gives us confidence that our a priori assumption of in situ and reworked is correct (Table 1).

5. Discussion

5.1 Updated age model

The age model for DSDP Site 274 is updated with four additional biostratigraphic datums and five magnetostratigraphic datums. Specifically, age constraints in the bottom (early Oligocene, 33.7 Ma, 404.66 mbsf) and top (late Oligocene, 24.4 Ma, 181.23 mbsf) of the studied interval (408.5–174.2 mbsf) have been improved. However, the few existing age constraints for the middle part (mid Oligocene, 307.1–199.5 mbsf) do not allow a significant improvement of the existing age model for this interval (Fig. 2b, Table 2). Jovane et al., (2020) presented an update of the biostratigraphic constrains of Site 274, and afterwards guided their magnetostratigraphic correlation with these constraints. Like ours, their polarity pattern alone is not sufficient to provide an independent chronology. Our obtained polarity pattern is similar to Jovane et al., (2020) for the upper part of our study, i.e. late Oligocene (Fig. 2b). This is also true for the unclear polarity zone between cores 29 and 25 where Jovane et al., (2020) also find inclinations that produce a uncertain polarity pattern. Our correlation with the time scale however differs in the lower part of the section, below 320 mbsf, where we provide new magnetostratigraphic data and biostratigraphic age constraints, and implement the most recent insights on the age of the ocean crust underlying the site (Cande et al., 2000). This results in younger ages for the lower part of the section, which are propagated upwards, altogether indicating younger ages for DSDP Site 274 than the study of Jovane et al. (2020) and the initial report. We acknowledge that although our new constraints have improved the age model, large uncertainties remain, due to moderate recovery, reworked material, weak NRM intensities (Table

S1) and limited occurrence of age-diagnostic microfossils. This means that between tie points, sedimentation rates may vary and hiatuses could be present. We therefore plot the data in the depth domain, and indicate the age tie points next to the depth scale (Fig. 2; Fig. 4). Notwithstanding these age model uncertainties, the proxy data we present provides a rare glimpse into early to middle Oligocene surface water conditions.

5.2 Paleotemperature and paleoenvironment in the Oligocene at DSDP Site 274

Temperature, in situ- and reworked palynomorph results together provide integrated paleoceanographic configurations offshore the Ross Sea margin during the Oligocene (33.7–24.4 Ma) (Fig. 4). Furthermore, we combine our reconstruction with those available around the East Antarctic margin from the Western Ross Sea and the Wilkes Land to obtain a regional perspective.

5.2.1 Surface oceanographic conditions

Both dinocyst assemblages and TEX_{86}- based SST results (Fig. 4b, c) consistently suggest temperate surface-ocean conditions. High variability in the dinocyst- and TEX_{86}-SST reconstructions reflects highly dynamic surface-ocean conditions. Although P-cyst species are abundant in the top and bottom of the record suggesting nutrient-rich conditions, the middle part of the record is dominated by high abundance of G-cyst species indicating that oligotrophic and warm conditions prevailed (Fig. 4b). The dominance of G-cysts implies that upwelling (the proto-Antarctic Divergence) was greatly reduced or located far away from the site. Above 265 mbsf, the more frequent shifts between P-cyst dominated and G-cyst dominated assemblages, reflects strongly varying oceanographic conditions, perhaps as a result of shifting frontal system locations or dynamics (as offshore Wilkes Land; Salabarnada et al., 2018; Bijl et al., 2018; Hartman et al., 2018). The scarce presence of typical sea-ice affiliated dinocysts suggests that sea ice was absent or the sea ice seasonal coverage was strongly reduced (Bijl et al., 2018) compared to the present-day (Fetterer et al., 2020). The dinocyst assemblages mostly contain known marine species, indicative of normal ocean salinities. However, Dinocyst sp. 1 (turquoise in Fig. 4b), abundant in sediments > 335 mbsf, morphologically resembles the peridinioid *Senegalinium* spp., a genus known for its high tolerance to low surface water salinities (Sluijs et al., 2009). If morphology is indicative of environmental conditions, the region could have been under the influence of meltwater and/or increased precipitation during the early Oligocene. The overall abundance of reworked (Eocene) dinocysts suggests erosion of marine sediments on the Ross Sea continental shelf, and transport thereof towards the abyssal plain by wind-driven transport of surface water or through density-driven bottom water flow cascading down the continental slope. In general, the Oligocene dinocyst assemblages found at DSDP Site 274, are similar to present-day dinocyst assemblages living between the Subantarctic and Subtropical front, where temperatures range from 0–15°C (Prebble et al., 2013). This is in line with the high TEX_{86}-SSTs (10–17°C), which indicates much warmer surface waters with lower nutrient levels than today where currently, the site is located in an area with average SSTs ~ -1°C (Locarnini et al., 2019).

5.2.2 Oligocene oceanography and climate evolution at DSDP Site 274 in a regional context

The generally warm SSTs throughout the Oligocene suggest that the recorded high productivity at the site was probably not the result of cold upwelled waters. Yet, in the early Oligocene (404.66–335.34 mbsf) the relative abundant P-cysts do indicate high nutrient and, possibly, low salinity surface-water conditions (Fig. 4b). Instead

of upwelling, we suggest that strong surface-water mixing stimulated ocean primary productivity at the site, perhaps with additional nutrient sources through melting from the Ross Sea continental margin. Rifting of the Western Ross Sea shelf since 60 Ma (Huerta and Harry, 2007) created thick Eocene sedimentary successions on the Ross Sea shelf. Glacial-isostatic adjustments as a response of the Antarctic ice sheet build-up (~48–34 Ma) caused reorganisation of shelf sedimentation (Stocchi et al., 2013), notably increases in sedimentation rates due to the accumulation space created by higher sea level and bedrock subsidence in some regions, and erosion due to bedrock uplift at others. Strata drilled at DSDP Site 270 on the Ross Sea continental shelf indicate periods of early Oligocene glacimarine deposition derived from local ice caps nucleated on elevated highs prior to tectonic subsidence in that region (De Santis 1999; Kulhanek et al., 2019). Turbid meltwater derived from the margins of these marine terminating ice caps, and from glacio-marine/fluvial systems at the margins of outlet glacier along the Transantarctic Mountain front (Fielding et al., 2000), would also allow for transport via a suspended sediment load or downslope processes towards the continental rise at DSDP Site 274, similar to the Wilkes Land continental rise (Bijl et al., 2018b; Salabarnada et al., 2018). The high abundance of reworked late Eocene dinocysts testifies to the influence of continental shelf-derived surface water towards the site, which brings nutrients and promotes productivity (increase in P cysts). This high amount of reworked dinocysts could further argue for a reworked TEX_{86}-SST signal. However, the near-shore character of the Eocene reworking (abundant pro-deltaic, marginal-marine peridinioid cysts) would have increased the branched, soil-derived GDGTs. This sharply contradicts with the low (<0.08) BIT values (Fig. S2). After ~29 Ma (335 mbsf), the relatively high TEX_{86}-based SSTs (10–17°C) and abundant offshore, temperate dinocyst species *Operculodinium* spp., *Spiniferites* spp., and *Nematosphaeropsis labyrinthus* (Fig.5b, c) indicate a long period of temperate conditions at DSDP Site 274. The covarying trend between dinocyst species and the SSTs indicates that SST has a strong influence on the biotic response.

For the first time *Malvinia escutiana* is found in mid Oligocene sediment (<265 mbsf), which extends the LO of this species relative to previous reports (Bijl et al., 2018a). Its high abundance suggests that conditions were favourable for this species, and makes it unlikely that its occurrence in the mid Oligocene represents a reworked signal. The CA plot (Fig. 3) shows that *Malvinia escutiana* co-varies with oligotrophic and temperate dinocyst groups as well as with acritarchs. This suggests that *Malvinia* favours open water and low nutrient conditions. A conundrum in our data is the increase in the G-cysts groups in the mid-Oligocene: *Batiacasphaera* spp., *Pyxidinopsis* spp. and *Cerebrocysta* spp., and a decrease in P-cyst abundances synchronous with declining SST starting at ~29 Ma (335.3 mbsf). At present, these G-cysts are associated with more northerly Subantarctic and Subtropical front zone regions (Prebble et al., 2013), with temperate ocean conditions. Although, in general, temperate dinocyst and lipid biomarker signals are consistent in the record, between ~29 Ma and 26.8 Ma (335.3–252.2 mbsf) an increase in warm-affiliated G-cyst assemblages corresponds to a decrease in SST. We here argue that decreasing nutrient levels cause P-cyst to be replaced by G-cysts. Throughout the record, variability in nutrient conditions rather than temperature seems to be the driving factor in dinocyst distribution.

Abundance of transparent chorate acritarchs at DSDP Site 274 generally follows warmer SSTs, similarly to what was found in the record of Site U1356 offshore Wilkes Land (Bijl et al., 2018b). The CA analysis showed little co-variance between acritarchs and reworked cysts, thus suggesting that the acritarchs are in situ. At ~26.5 Ma

(239.2 mbsf) the acritarchs peak is synchronous with a peak in temperate dinocyst species *Operculodinium* spp. Acritarchs as well as *Operculodinium* spp. a pioneer species, is known to be opportunist (e.g., Dale, 1996). Previous studies on Antarctic proximal records, from the CIROS-1 core (Hannah, 1997) and DSDP Site 270 (Kulhanek et al., 2019), have associated the presence of acritarchs (*Leiosphaeridia* spp.) and prasinophytes (*Cymatiosphaera* spp.) with episodes of sea ice melting. We did not find abundant *Leiosphaeridia* spp. Thus we interpret that the melt-water influence was reduced at DSDP Site 274, compared to sites on the Ross Sea continental shelf that were more proximal to the glaciated margin.

5.3 Regional perspective

We compare our Oligocene paleoceanographic reconstructions from DSDP Site 274 with records from off the Wilkes Land margin (Site U1356 (Hartman et al., 2018; Salabarnada et al., 2018; Bijl et al., 2018a, b; Sangiorgi et al., 2018)) and the Ross Sea; (Houben et al., 2013; Clowes et al., 2016; Kulhanek et al., 2019; Duncan, 2017) (Fig. 5). Published TEX_{86} data from Wilkes Land margin (Hartman et al., 2018) and the Ross Sea (Duncan, 2017) have for this comparison been converted to SSTs using linear calibration of Kim et al. (2010) (calibration error: ± 5.2°C).

Early Oligocene (32.3–29.2 Ma, 391–335 mbsf)

DSDP Site 274 TEX_{86}-SST results suggest a slightly lower average temperature offshore the Ross Sea (~4°C) than at Wilkes Land (Site U1356), but higher temperatures (~6°C) than at ice proximal Ross Sea site (CIROS-1; Fig. 5c). This observation is consistent with the position of DSDP Site 274, which was at higher paleo-latitudes compared to Site U1356, and but lower latitudes and offshore the ice proximal sites within the Ross Sea. Indeed, evidence from the CRP cores in the Ross Sea showed continental-scale ice sheets first expanded towards the Ross Sea around 32.8 Ma (Galeotti et al., 2016). Prior to 31 Ma (350 mbsf), the SST record from DSDP Site 274 shows some of its highest temperatures, while SSTs at Site U1356 decrease. One important consideration is whether these sites in the Ross Sea and Wilkes Land can be compared as belonging to a latitudinal transect, given that they are separated by an evolving Tasmanian Gateway, a conduit that separates the eastern Indian and southwestern Pacific oceans. Although a deep-water connection in the Tasmanian Gateway was established in the Oligocene, the passageway was still restricted (Stickley et al., 2004; Bijl et al., 2013). Studies of the paleobathymetry and sedimentary mechanisms in the Southern Ocean through the Cenozoic (e.g., Scher et al., 2015; Hochmuth et al., 2020) do show the Tasmanian Gateway as well as the Pacific sector of the Southern Ocean deepen between 34 Ma and 27 Ma, allowing easier throughflow and exchange between the different ocean sectors. The limited co-variability between the Adare Basin and Wilkes Land margin, and the different SSTs might signal the disconnection between the two sites, perhaps by a still restricted Tasmanian Gateway. While synchronous SST variability and changes therein between the sectors after 31 Ma suggests connection between the ocean basins, in line with other studies (Scher et al., 2015), a SST difference between both sectors remains. The abundance of low nutrient/temperate-affiliated dinocyst taxa (G-cyst) is higher at DSDP Site 274 than at the Wilkes Land margin and within the Ross Sea continental shelf, implying that nutrient input was lower at the offshore Ross Sea location than at more proximal sites, with a higher degree of melt water input.

Latest early Oligocene to earliest late Oligocene: "Mid Oligocene" (29.1–26.6 Ma, 333.6 – 239 mbsf)

In the "mid Oligocene", the absolute SST average values disparity between DSDP Site 274, the Ross Sea and Wilkes Land margin is the strongest. Both Wilkes Land margin and the Ross Sea have high P-cyst content (Fig. 5b). Palynomorphs from Ross Sea shelf deposits from Oligocene, dominated by *Lejeunecysta* spp. and brackish water prasinophyte *Cymatiosphaera* (CRP: Prebble et al., 2006; Clowes et al., 2016), suggest meltwater input in the Ross Sea region through this time interval (Prebble et al., 2006). In contrast, our dinocyst assemblages suggest pelagic, low nutrient, marine conditions while the low numbers of terrestrial palynomorphs point to limited fresh-water or melt-water input at DSDP Site 274. Similar to the Wilkes Land margin SST record, DSDP Site 274 SSTs decrease towards the late Oligocene.

Late Oligocene (26.5 – ~24.4 Ma, 239-192.7 mbsf)

The average TEX_{86}-based SST results (Fig. 5a) for Site U1356 and DSDP Site 274 shows large (>6°C) temperature variability (Hartman et al., 2018). At DSDP Site 274, we can exclude the known non-thermal biases as cause for the strong variability (Fig. S2), and therefore also interpret stronger SST variability in the late Oligocene. Noteworthy, in the beginning of this interval at 26.5 Ma (239 mbsf) we see a temperature peak at DSDP Site 274 similar to what was reconstructed at the Wilkes Land margin (Hartman et al., 2018). This temperature peak coincides with a rapid decrease in the $\delta^{18}O$ isotope records that may be linked to the deglaciation of large parts of the Antarctic ice sheet following a large transient glaciation centered on ~26.8 Ma (Pälike et al., 2006). The increase in abundance of *Operculodinium* spp. at all three sites (DSDP Sites 270, 274 and IODP Site U1356) is a testament to the temperate conditions and/or lower nutrient availability at the time. The DSDP Site 274 sediment record is virtually barren of palynomorphs <192.7 mbsf (~24.4 Ma), 11.7 m below the hiatus (181 mbsf) in the record, with the sediments above estimated to be of middle Miocene age (Hayes et al., 1975). Since our SST reconstructions exclude continuous sea ice cover as possible explanation, we interpret that oxic degradation consumed palynomorphs at the sea floor. Three reasons for increased oxygen delivery at the sea floor are proposed; 1. Strengthening of the Antarctic Circumpolar Current (ACC) increased deep ventilation. This is unlikely given that ocean frontal systems would progressively move northward while the Tasmanian Gateway widens, which would also displace ACC flow northwards, away from the site. 2. Winnowing ocean bottom currents and decreased sedimentation rates could cause the oxic conditions we propose, and was the reason behind the disappearance of dinocysts. However, winnowing would not erode palynomorphs only and would result in coarsening of sediments, which we do not see. The lithology of the 192.7–181 mbsf interval where dinocyst are barren, is diatom rich silty-clay. Decreased sedimentation rates would prolong oxygen exposure time of palynomorphs once at the sea floor. Although our age model has limitations, a decrease in sedimentation rates (to 1.8 cm/kyr) is observed above 192.7 mbsf. 3. Bottom water formation on the Ross Sea continental margin delivered increased oxygen-rich bottom waters to the site. Heightened obliquity sensitivity has been interpreted to be associated with enhanced oceanic-influence mass balance controls on marine terminating ice sheets, with limited sea ice extent (Levy et al., 2019). Levy et al. (2019) interpreted a prominent increase in the sensitivity of benthic oxygen isotope variations to obliquity forcing (termed "obliquity sensitivity") between 24.5 and 24 Ma, synchronous with the first occurrence of ice-proximal glaciomarine sediments at DSDP Site 270, disconformities in CRP-2/2A, and a large turnover in Southern Ocean phytoplankton. The major expansion of the ice sheet close to the Oligocene – Miocene boundary in the Ross Sea (Levy et al., 2019; Kulhanek et al., 2019; Evangelinos et al., in review) argues in favour of Ross Sea bottom water strengthening, leading to the slow-down of the sedimentation rates above 192.7 mbsf and the formation of the >7 Myr duration hiatus at ~181 mbsf.

5.4 Implications for ice-proximal conditions, hydrology and ice sheets: a hypothesis

Warm and generally oligotrophic conditions relatively proximal to the Antarctic margin during the Oligocene, imply that the Southern Ocean oceanography was fundamentally different from modern (e.g., Deppeler and Davidson, 2017). Although our data suggest ocean conditions were colder inshore than further offshore, they remain warm considering their proximity to marine-terminating outlet glaciers and ice caps in the Ross Sea area (De Santis et al 1999; Galeotti et al., 2016; Levy et al., 2019; Kulhanek et al., 2019; Evangelinos et al., in review). Levy et al. (2019) provided a model for ice-proximal to ice-distal oceanographic conditions in the Ross Sea during the Oligocene. In that model, Transantarctic Mountain outlet glaciers draining the EAIS, or local marine-terminating ice caps in the Ross Sea were particularly affected by the wind-driven, southward advection of warmer subsurface waters onto the Ross Sea shelf, similar to how Circumpolar Deep Water is being transported onto some regions of the continental shelf today (e.g., Wouters et al., 2015; Shen et al., 2018). The subsurface waters in that conceptual model were indicated as warmer than the overlying low salinity surface waters derived from glacial melts during glacial maxima, but this stratification is broken down during interglacials. The sample resolution of our dataset is too low to capture the full amplitude of orbital variability. However, since each 2 cm sample represents 800 yrs, the variability we see in our record could be the result of strong environmental variability on orbital time scales. Hence, the high variability in our data support the interpretation of Levy et al., 2019, with temperate surface waters at DSDP Site 274 on the continental rise of the Ross Sea margin suggesting a well-mixed water column as it would be difficult to envisage intermediate waters warmer than the surface waters. In this scenario, colder stratified surface water due to (sea ice) melting would be largely restricted to coastal Ross Sea sites of DSDP Site 270, CRP and CIROS-1. Temperate surface waters offshore the Ross Sea shelf would provide a source of heat that limits the advance of marine terminating glacial systems into the Ross Sea and Wilkes Land continental shelfs. Pollen assemblages and high SSTs at DSDP Site 274, supported by terrestrial palynomorphs found at CRP-2 (Askin and Raine, 2000), suggest that climate was warm enough to allow atmospheric melt to be the dominant control on the ice mass balance and potential driver of deglaciation during warm orbital configurations. In addition, the warm ocean could have promoted an intensification of the hydrological cycle and consequent moisture delivery to the Antarctic hinterland, similar to what has been hypothesised for the Miocene Climatic Optimum (Feakins et al., 2012). Enhanced intense precipitation in the Antarctic hinterland would favour ice accumulation during cold orbital states to sustain a marine termination for the predominately terrestrial ice sheets. In a warmer-than-present climate of the early to mid Oligocene, precipitation and glaciation on the hinterlands could be further promoted by high elevation and larger Antarctic landmass size (Paxman et al., 2019). Indeed, General Circulation Models (GCMs) for the ice-free Eocene do suggest enhanced precipitation delivery to the Antarctic continent (e.g., Huber and Caballero, 2011; Baatsen et al., 2018). If part of the source of that precipitation was the warm Southern Ocean proximal to the ice sheet, Rayleigh distillation would be reduced, leading to relatively enriched Oligocene ice sheet $\delta^{18}O$ compared to that of today, and thereby, relatively depleted sea water $\delta^{18}O$. The calculation of ice volumes from benthic foraminiferal oxygen isotope records (e.g., Lear et al., 2000; Bohaty et al., 2012; Liebrand et al., 2017) do consider a variety of values for the isotopic composition of Oligocene Antarctic ice sheet. We argue that the warm oceanographic conditions, invoking strong precipitation and possible more local source of precipitation than today (Speelman et al., 2010), would explain how $\delta^{18}O$ of Antarctic ice was on the less depleted end of previous assumptions. This increases the calculated Antarctic ice mass that was installed during the EOIS (Bohaty et al., 2012), and the Antarctic ice volume that fluctuated over

strong Oligocene orbital cycles (Liebrand et al., 2017). This idea could in the future be further tested through higher resolution reconstructions, δD reconstructions on plant matter and isotope-enabled paleoceanographic and ice sheet modelling studies. In any case, future isotope-enabled ice sheet modelling should factor in warm Southern Ocean conditions for realistic estimates of Antarctic ice volume. This may imply an even higher sensitivity of Antarctic ice sheets to orbitally forced climate variability than previously assumed, and assigns a large role of mass balance controlled by surface melt and oceanography in ice sheet stability during past warm climates, through both hydrological and basal and surface melt processes.

6. Conclusion

We show that temperate (TEX_{86}-SST: 10–17°C ± 5.2°C) and relatively oligotrophic surface ocean conditions prevailed off the Ross Sea margin during the Oligocene (33.7–24.4 Ma). This agrees with the warm SSTs recorded offshore Wilkes Land, and demonstrates that warm surface waters influenced the East Antarctic Ice Sheet margin in both the Ross Sea and Wilkes Land during the Oligocene. The warm surface ocean temperatures at DSDP Site 274 and colder SST in the Ross Sea continental shelf with evidence of temporary marine termination of ice caps and glaciers demonstrate a strong inshore to offshore temperature gradient at the Ross Sea. We posit that the warm surface ocean conditions near the continental shelf break during the Oligocene may have promoted increased heat delivery and precipitation transport towards the Antarctic hinterlands that lead to highly dynamic terrestrial ice sheet volumes in the warmer climate state of the Oligocene. During cold orbital phases, enhanced precipitation may have sustained high ice flux and advance of terrestrial ice sheet and ice caps into shallow marine settings. During warm orbital configurations of the Oligocene, the heat delivery may have resulted in widespread surface melt and retreat of the terrestrial ice sheets into the hinterland.

Acknowledgements

This work used Deep Sea Drilling Project archived samples and data provided and curated by the International Ocean Discovery Program and its predecessors. This study was funded by NWO polar programme grant number ALW.2016.001. DE acknowledges funding through the Alexander S. Onassis Public Benefit Foundation Ph.D. research grant: F ZL 016-1/2015-2016. DE and CE acknowledge funding through the Spanish Ministry of Economy, Industry and Competitivity (grant CTM2017-89711-C2-1-P/ CTM2017-89711-C2-2-P), co-funded by the European Union through FEDER funds. We thank the Paleomagnetic Laboratory CCiTUB-ICTJA CSIC for the support on paleomagnetic analysis. We thank Natasja Welters and Giovanni Dammers for technical support at the Utrecht University GeoLab.

Author contributions

PKB and FS designed the research. PKB, CE and DE collected the samples. CE and DE described the cores. LV collected and analysed paleomagnetic samples. FSH processed samples for palynology and organic geochemistry, FSH, PKB and FS interpreted the data. FSH wrote the paper with input from all authors.

References

Askin, R. and Raine, J.: Oligocene and Early Miocene terrestrial palynology of the Cape Roberts Drillhole CRP-2/2A, Victoria Land Basin, Antarctica, Terra Antartica, 7, 493-501, 2000.

Barrett, P. J.: Antarctic Cenozoic history from the CIROS-1 drillhole, McMurdo Sound, DSIR Pub., 1989.

Bijl, P. K., Pross, J., Warnaar, J., Stickley, C. E., Huber, M., Guerstein, R., Houben, A. J., Sluijs, A., Visscher, H., and Brinkhuis, H.: Environmental forcings of Paleogene Southern Ocean dinoflagellate biogeography, Paleoceanography, 26, 2011.

Bijl, P. K., Bendle, J. A., Bohaty, S. M., Pross, J., Schouten, S., Tauxe, L., Stickley, C. E., McKay, R. M., Röhl, U., and Olney, M.: Eocene cooling linked to early flow across the Tasmanian Gateway, Proceedings of the National Academy of Sciences, 110, 9645-9650, 2013.

Bijl, P. K., Houben, A. J., Bruls, A., Pross, J., and Sangiorgi, F.: Stratigraphic calibration of Oligocene-Miocene organic-walled dinoflagellate cysts from offshore Wilkes Land, East Antarctica, and a zonation proposal, Journal of Micropalaeontology, 37, 105-138, 2018a.

Bijl, P. K., Houben, A. J., Hartman, J. D., Pross, J., Salabarnada, A., Escutia, C., and Sangiorgi, F.: Paleoceanography and ice sheet variability offshore Wilkes Land, Antarctica-Part 2: Insights from Oligocene-Miocene dinoflagellate cyst assemblages, Climate of the Past, 14, 1015-1033, 2018b.

Baatsen, M., von der Heydt, A., Huber, M., Kliphuis, M. A., Bijl, P. K., Sluijs, A., and Dijkstra, H. A.: Equilibrium state and sensitivity of the simulated middle-to-late Eocene climate, Clim. Past Discuss, 2018, 1-49, 2018.

Blaga, C. I., Reichart, G.-J., Heiri, O., and Damsté, J. S. S.: Tetraether membrane lipid distributions in water-column particulate matter and sediments: a study of 47 European lakes along a north–south transect, Journal of Paleolimnology, 41, 523-540, 2009.

Bohaty, S. M., Zachos, J. C., and Delaney, M. L.: Foraminiferal Mg/Ca evidence for southern ocean cooling across the eocene–oligocene transition, Earth and Planetary Science Letters, 317, 251-261, 2012.

Burns, D. A.: Nannofossil biostratigraphy for Antarctic sediments, Leg 28, Deep Sea Drilling Project, 1975.

Cande, S. C., Stock, J. M., Müller, R. D., and Ishihara, T.: Cenozoic motion between east and west Antarctica, Nature, 404, 145, 2000.

Church, M. J., DeLong, E. F., Ducklow, H. W., Karner, M. B., Preston, C. M., and Karl, D. M.: Abundance and distribution of planktonic Archaea and Bacteria in the waters west of the Antarctic Peninsula. Limnology and Oceanography, 48(5), 1893-1902, 2003.

Clowes, C. D., Hannah, M. J., Wilson, G. J., and Wrenn, J. H.: Marine palynostratigraphy and new species from the Cape Roberts drill-holes, Victoria land basin, Antarctica, Marine Micropaleontology, 126, 65-84, 2016.

Coxall, H. K., Wilson, P. A., Pälike, H., Lear, C. H., and Backman, J.: Rapid stepwise onset of Antarctic glaciation and deeper calcite compensation in the Pacific Ocean, Nature, 433, 53-57, 2005.

Cramwinckel, M. J., Woelders, L., Huurdeman, E. P., Peterse, F., Gallagher, S. J., Pross, J., Burgess, C. E., Reichart, G. J., Sluijs, A., and Bijl, P. K.: Surface-circulation change in the southwest Pacific Ocean across the Middle Eocene Climatic Optimum: inferences from dinoflagellate cysts and biomarker paleothermometry, Clim. Past, 16, 1667-1689, 2020.

Crouch, E. M., Willumsen, P. S., Kulhanek, D. K., and Gibbs, S. J.: A revised Paleocene (Teurian) dinoflagellate cyst zonation from eastern New Zealand, Review of Palaeobotany and Palynology, 202, 47-79, 2014.

Crouch, E., Shepherd, C., Morgans, H., Naafs, B., Dallanave, E., Phillips, A., Hollis, C., and Pancost, R.: Climatic and environmental changes across the early Eocene climatic optimum at mid-Waipara River, Canterbury Basin, New Zealand, Earth-Science Reviews, 200, 102961, 2020.

Dale, B.: Dinoflagellate cyst ecology: modeling and geological applications, Palynology: principles and applications, 1996. 1249-1275, 1996.

Deppeler, S. L. and Davidson, A. T.: Southern Ocean phytoplankton in a changing climate, Frontiers in Marine Science, 4, 40, 2017.

De Santis, L., Anderson, J. B., Brancolini, G., and Zayatz, I.: Seismic record of late Oligocene through Miocene glaciation on the central and eastern continental shelf of the Ross Sea, in Geology and Seismic Stratigraphy of the Antarctic Margin, Antarct. Res. Ser., vol. 68, edited by A. K. Cooper, P. F. Barker, and G. Brancolini, AGU, Washinghton, D. C, pp. 235–260, 1995.

De Santis, L., Prato, S., Brancolini, G., Lovo, M., and Torelli, L.: The Eastern Ross Sea continental shelf during the Cenozoic: implications for the West Antarctic ice sheet development, Global and Planetary Change, 23, 173-196, 1999.

De Schepper, S., Fischer, E. I., Groeneveld, J., Head, M. J., and Matthiessen, J.: Deciphering the palaeoecology of Late Pliocene and Early Pleistocene dinoflagellate cysts, Palaeogeography, Palaeoclimatology, Palaeoecology, 309, 17-32, 2011.

Duncan, B.: Cenozoic Antarctic climate evolution based on molecular and isotopic biomarker reconstructions from geological archives in the Ross Sea region, 2017.

Egger, L. M., Bahr, A., Friedrich, O., Wilson, P. A., Norris, R. D., Van Peer, T. E., Lippert, P. C., Liebrand, D., and Pross, J.: Sea-level and surface-water change in the western North Atlantic across the Oligocene–Miocene Transition: a palynological perspective from IODP Site U1406 (Newfoundland margin), Marine Micropaleontology, 139, 57-71, 2018.

Escutia, C., Brinkhuis, H., and Klaus, A.: IODP Expedition 318: From Greenhouse to Icehouse at the Wilkes Land Antarctic Margin, Scientific Drilling, 2011.

Evangelinos, D., Escutia, C., van de Flierd, T., Valero L., Hoem, F., Bijl, P., Flores, J.A., Harwood, D.M., Etourneau J., Katharina, Kreissig, K., Nilsson-Kerri, K., Holder, L., López-Quirós, A., Salabarnada, A.: Absence of a strong, deep-reaching Antarctic Circumpolar Current zonal flow across the Tasmanian Gateway during the Oligocene-early Miocene. *Earth and Planetary Science Letters* (submitted). 2020.

Evangelinos D., Escutia C., Etourneau, J., Hoem F., Bijl P., Boterblom W., van de Flierdt T., Valero L., Flores J-A., Rodriguez-Tovar F.J., Jimenez-Espejo F.J., Salabarnada A., López-Quirós A.: Late Oligocene-Miocene proto-Antarctic Circumpolar Current dynamics off the Wilkes Land margin, East Antarctica. Global and Planetary Change, 103221. 2020

Feakins, S. J., Warny, S., and Lee, J.-E.: Hydrologic cycling over Antarctica during the middle Miocene warming, Nature Geoscience, 5, 557-560, 2012.

Fetterer, F., Knowles, K., Meier, W., Savoie, M., and Windnagel, A.: Updated daily. Sea ice index, version 3. Boulder, Colorado USA. NSIDC: National Snow and Ice Data Center, 2020.

Fielding, C.R., Naish, T.R., Woolfe, K.J., Lavelle, M.: Facies analysis and sequence stratigraphy of CRP-2/2A, Victoria Land basin, Antarctica. Terra Antartica 7, 323–338, 2000.

Frieling, J. and Sluijs, A.: Towards quantitative environmental reconstructions from ancient non-analogue microfossil assemblages: Ecological preferences of Paleocene–Eocene dinoflagellates, Earth-Science Reviews, 185, 956-973, 2018.

Galeotti, S., DeConto, R., Naish, T., Stocchi, P., Florindo, F., Pagani, M., Barrett, P., Bohaty, S. M., Lanci, L., and Pollard, D.: Antarctic Ice Sheet variability across the Eocene-Oligocene boundary climate transition, Science, 352, 76-80, 2016.

Gombos, A. M. and AM JR, G.: Paleogene and Neogene diatoms from the Falkland Plateau and Malvinas Outer Basin: Leg 36, Deep Sea Drilling Project, 1977.

Gradstein, F. M., Ogg, J. G., Schmitz, M., and Ogg, G.: The geologic time scale 2012, elsevier, 2012.

Granot, R., Cande, S., Stock, J., Davey, F., and Clayton, R.: Postspreading rifting in the Adare Basin, Antarctica: regional tectonic consequences, Geochemistry, Geophysics, Geosystems, 11, 2010.

Hammer, Ø., Harper, D., and Ryan, P.: PAST—PAlaeontological STatistics, ver. 3.15, https://folk. uio. no/ohammer/past/Acesso em, 23, 2017, 2001.

Hannah, M.: Climate controlled dinoflagellate distribution in late Eocene-earliest Oligocene strata from CIROS-1 Drillhole, McMurdo Sound, Antarctica, Terra Antartica, 4, 73-78, 1997.

Hartman, J. D., Sangiorgi, F., Salabarnada, A., Peterse, F., Houben, A. J., Schouten, S., Brinkhuis, H., Escutia, C., and Bijl, P. K.: Paleoceanography and ice sheet variability offshore Wilkes Land, Antarctica-Part 3: Insights from Oligocene-Miocene TEX86-based sea surface temperature reconstructions, Climate of the Past, 14, 1275-1297, 2018.

Hayes, D. E., Frakes, L.A, Bar, P.J, Derek A Burns, Pei-hsin Chen, The Shipboard Scientific Party, et al., : 10. SITE 274 The Shipboard Scientific Party 1 SITE DATA, 28, 1975.

Ho, S. L., Mollenhauer, G., Fietz, S., Martínez-Garcia, A., Lamy, F., Rueda, G., Schipper, K., Méheust, M., Rosell-Melé, A., and Stein, R.: Appraisal of TEX86 and TEX86L thermometries in subpolar and polar regions, Geochimica et Cosmochimica Acta, 131, 213-226, 2014.

Hochmuth, K., Gohl, K., Leitchenkov, G., Sauermilch, I., Whittaker, J. M., Uenzelmann-Neben, G., Davy, B., and De Santis, L.: The evolving paleobathymetry of the circum-Antarctic Southern Ocean since 34 Ma–a key to understanding past cryosphere-ocean developments, Geochemistry, Geophysics, Geosystems, 2020.

Hopmans, E. C., Weijers, J. W., Schefuß, E., Herfort, L., Damsté, J. S. S., and Schouten, S.: A novel proxy for terrestrial organic matter in sediments based on branched and isoprenoid tetraether lipids, Earth and Planetary Science Letters, 224, 107-116, 2004.

Hopmans, E. C., Schouten, S., and Damsté, J. S. S.: The effect of improved chromatography on GDGT-based palaeoproxies, Organic Geochemistry, 93, 1-6, 2016.

Houben, A. J., Bijl, P. K., Guerstein, G. R., Sluijs, A., and Brinkhuis, H.: Malvinia escutiana, a new biostratigraphically important Oligocene dinoflagellate cyst from the Southern Ocean, Review of Palaeobotany and Palynology, 165, 175-182, 2011.

Houben, A. J., Bijl, P. K., Pross, J., Bohaty, S. M., Passchier, S., Stickley, C. E., Röhl, U., Sugisaki, S., Tauxe, L., and van de Flierdt, T.: Reorganization of Southern Ocean plankton ecosystem at the onset of Antarctic glaciation, Science, 340, 341-344, 2013.

Houben, A. J., Bijl, P. K., Sluijs, A., Schouten, S., and Brinkhuis, H.: Late Eocene Southern Ocean cooling and invigoration of circulation preconditioned Antarctica for full-scale glaciation, Geochemistry, Geophysics, Geosystems, 2019.

Huber M, Caballero R. The early Eocene equable climate problem revisited. Climate of the Past, 2011.

Huerta, A. D. and Harry, D. L.: The transition from diffuse to focused extension: Modeled evolution of the West Antarctic Rift system, Earth and Planetary Science Letters, 255, 133-147, 2007.

Jovane, L., Florindo, F., Wilson, G., Leone, S. d. A. P. S., Hassan, M. B., Rodelli, D., and Cortese, G.: Magnetostratigraphic Chronology of a Cenozoic Sequence From DSDP Site 274, Ross Sea, Antarctica, Multi-Disciplinary Applications in Magnetic Chronostratigraphy, 2020.

Juggins, S.: C2: Software for ecological and palaeoecological data analysis and visualisation (user guide version 1.5), Newcastle upon Tyne: Newcastle University, 77, 2007.

Kalanetra, K. M., Bano, N., and Hollibaugh, J. T.: Ammonia-oxidizing Archaea in the Arctic Ocean and Antarctic coastal waters. Environmental Microbiology, 11(9), 2434-2445, 2009.

Kim, J.-H., Van der Meer, J., Schouten, S., Helmke, P., Willmott, V., Sangiorgi, F., Koç, N., Hopmans, E. C., and Damsté, J. S. S.: New indices and calibrations derived from the distribution of crenarchaeal isoprenoid tetraether lipids: Implications for past sea surface temperature reconstructions, Geochimica et Cosmochimica Acta, 74, 4639-4654, 2010.

Kim, J. H., Crosta, X., Willmott, V., Renssen, H., Bonnin, J., Helmke, P., Schouten, S., and Sinninghe Damsté, J. S.: Holocene subsurface temperature variability in the eastern Antarctic continental margin, Geophysical Research Letters, 39, 2012.

Kulhanek, D. K., Levy, R. H., Clowes, C. D., Prebble, J. G., Rodelli, D., Jovane, L., Morgans, H. E., Kraus, C., Zwingmann, H., and Griffith, E. M.: Revised chronostratigraphy of DSDP Site 270 and late Oligocene to early Miocene paleoecology of the Ross Sea sector of Antarctica, Global and Planetary Change, 178, 46-64, 2019.

Levy, R., Harwood, D., Florindo, F., Sangiorgi, F., Tripati, R., Von Eynatten, H., Gasson, E., Kuhn, G., Tripati, A., and DeConto, R.: Antarctic ice sheet sensitivity to atmospheric CO2 variations in the early to mid-Miocene, Proceedings of the National Academy of Sciences, 113, 3453-3458, 2016.

Levy, R. H., Meyers, S., Naish, T., Golledge, N., McKay, R., Crampton, J. S., DeConto, R., De Santis, L., Florindo, F., and Gasson, E. G.: Antarctic ice-sheet sensitivity to obliquity forcing enhanced through ocean connections, Nature Geoscience, 12, 132-137, 2019.

Liebrand, D., de Bakker, A. T., Beddow, H. M., Wilson, P. A., Bohaty, S. M., Ruessink, G., Pälike, H., Batenburg, S. J., Hilgen, F. J., and Hodell, D. A.: Evolution of the early Antarctic ice ages, Proceedings of the National Academy of Sciences, 114, 3867-3872, 2017.

Locarnini, R.A., A.V. Mishonov, O.K. Baranova, T.P. Boyer, M.M. Zweng, H.E. Garcia, J.R. Reagan, D. Seidov, K.W. Weathers, C.R. Paver, and I.V. Smolyar. World Ocean Atlas 2018, Volume 1: Temperature. A. Mishonov, Technical Editor. NOAA Atlas NESDIS 81, 52pp, 2019.

Marret, F., Bradley, L., de Vernal, A., Hardy, W., Kim, S.-Y., Mudie, P., Penaud, A., Pospelova, V., Price, A. M., and Radi, T.: From bi-polar to regional distribution of modern dinoflagellate cysts, an overview of their biogeography, Marine Micropaleontology, 2019. 101753, 2019.

Massana, R., Taylor, L. T., Murray, A. E., Wu, K. Y., Jeffrey, W. H., and DeLong, E. F.: Vertical distribution and temporal variation of marine planktonic archaea in the Gerlache Strait, Antarctica, during early spring. Limnology and Oceanography, 43(4), 607-617, 2009.

Macphail, M.: The Sabrina Microfloras of East Antarctica: Late Cretaceous Paleogene or reworked?, Palynology, 2021. 1-12, 2021.

McKay, R., Barrett, P., Levy, R., Naish, T., Golledge, N., and Pyne, A.: Antarctic Cenozoic climate history from sedimentary records: ANDRILL and beyond, Philosophical Transactions of the Royal Society A: Mathematical, Physical and Engineering Sciences, 374, 20140301, 2016.

Müller, R. D., Cannon, J., Qin, X., Watson, R. J., Gurnis, M., Williams, S., Pfaffelmoser, T., Seton, M., Russell, S. H., and Zahirovic, S.: GPlates: building a virtual Earth through deep time, Geochemistry, Geophysics, Geosystems, 19, 2243-2261, 2018.

Naish, T. R., Woolfe, K. J., Barrett, P. J., Wilson, G. S., Atkins, C., Bohaty, S. M., Bücker, C. J., Claps, M., Davey, F. J., and Dunbar, G. B.: Orbitally induced oscillations in the East Antarctic ice sheet at the Oligocene/Miocene boundary, Nature, 413, 719-723, 2001.

O'Brien, C. L., Huber, M., Thomas, E., Pagani, M., Super, J. R., Elder, L. E., and Hull, P. M.: The enigma of Oligocene climate and global surface temperature evolution, Proceedings of the National Academy of Sciences, 117, 25302-25309, 2020.

Orsi, A. H. and Wiederwohl, C. L.: A recount of Ross Sea waters, Deep Sea Research Part II: Topical Studies in Oceanography, 56, 778-795, 2009.

Pälike, H., Norris, R. D., Herrle, J. O., Wilson, P. A., Coxall, H. K., Lear, C. H., Shackleton, N. J., Tripati, A. K., and Wade, B. S.: The heartbeat of the Oligocene climate system, science, 314, 1894-1898, 2006.

Passchier, S., Ciarletta, D. J., Henao, V., and Sekkas, V.: Sedimentary processes and facies on a high-latitude passive continental margin, Wilkes Land, East Antarctica, Geological Society, London, Special Publications, 475, 181-201, 2019.

Paxman, G. J., Jamieson, S. S., Hochmuth, K., Gohl, K., Bentley, M. J., Leitchenkov, G., and Ferraccioli, F.: Reconstructions of Antarctic topography since the Eocene–Oligocene boundary, Palaeogeography, palaeoclimatology, palaeoecology, 535, 109346, 2019.

Pearson, A., Huang, Z., Ingalls, A., Romanek, C., Wiegel, J., Freeman, K. H., Smittenberg, R., and Zhang, C.: Nonmarine crenarchaeol in Nevada hot springs, Appl. Environ. Microbiol., 70, 5229-5237, 2004.

Pérez, L. F., De Santis, L., McKay, R. M., Larter, R. D., Ash, J., Bart, P. J., Böhm, G., Brancatelli, G., Browne, I., and Colleoni, F.: Early and middle Miocene ice sheet dynamics in the Ross Sea: Results from integrated core-log-seismic interpretation, GSA Bulletin, 2021.

Peterse, F., Kim, J.-H., Schouten, S., Kristensen, D. K., Koç, N., and Damsté, J. S. S.: Constraints on the application of the MBT/CBT palaeothermometer at high latitude environments (Svalbard, Norway), Organic Geochemistry, 40, 692-699, 2009.

Prebble, J., Crouch, E., Carter, L., Cortese, G., Bostock, H., and Neil, H.: An expanded modern dinoflagellate cyst dataset for the Southwest Pacific and Southern Hemisphere with environmental associations, Marine Micropaleontology, 101, 33-48, 2013a.

Prebble, J., Hannah, M., and Barrett, P.: Changing Oligocene climate recorded by palynomorphs from two glacio-eustatic sedimentary cycles, Cape Roberts Project, Victoria Land Basin, Antarctica, Palaeogeography, Palaeoclimatology, Palaeoecology, 231, 58-70, 2006.

Pritchard, H., Ligtenberg, S. R., Fricker, H. A., Vaughan, D. G., van den Broeke, M. R., and Padman, L.: Antarctic ice-sheet loss driven by basal melting of ice shelves, Nature, 484, 502-505, 2012.

Richey, J. N. and Tierney, J. E.: GDGT and alkenone flux in the northern Gulf of Mexico: Implications for the TEX86 and UK'37 paleothermometers, Paleoceanography, 31, 1547-1561, 2016.

Salabarnada, A., Escutia, C., Röhl, U., Nelson, C. H., McKay, R., Jiménez-Espejo, F., Bijl, P., Hartman, J., Strother, S., and Salzmann, U.: Paleoceanography and ice sheet variability offshore Wilkes Land, Antarctica–Part 1: Insights from late Oligocene astronomically paced contourite sedimentation, Climate of the Past, 14, 991-1014, 2018.

Sangiorgi, F., Bijl, P. K., Passchier, S., Salzmann, U., Schouten, S., McKay, R., Cody, R. D., Pross, J., Van De Flierdt, T., and Bohaty, S. M.: Southern Ocean warming and Wilkes Land ice sheet retreat during the mid-Miocene, Nature communications, 9, 317, 2018.

Scher, H. D., Bohaty, S. M., Zachos, J. C., and Delaney, M. L.: Two-stepping into the icehouse: East Antarctic weathering during progressive ice-sheet expansion at the Eocene–Oligocene transition, Geology, 39, 383-386, 2011.

Scher, H. D., Whittaker, J. M., Williams, S. E., Latimer, J. C., Ko- rdesch, W. E. C., and Delaney, M. L.: Onset of Antarctic Cir- cumpolar Current 30 million years ago as Tasmanian Gateway aligned with westerlies, Nature, 523, 580–583, 2015.

Schoof, C.: Ice sheet grounding line dynamics: Steady states, stability, and hysteresis, Journal of Geophysical Research: Earth Surface, 112, 2007.

Schouten, S., Hopmans, E. C., Rosell-Melé, A., Pearson, A., Adam, P., Bauersachs, T., Bard, E., Bernasconi, S. M., Bianchi, T. S., and Brocks, J. J.: An interlaboratory study of TEX86 and BIT analysis of sediments, extracts, and standard mixtures, Geochemistry, Geophysics, Geosystems, 14, 5263-5285, 2013.

Schouten, S., Hopmans, E. C., Schefuß, E., and Damste, J. S. S.: Distributional variations in marine crenarchaeotal membrane lipids: a new tool for reconstructing ancient sea water temperatures?, Earth and Planetary Science Letters, 204, 265-274, 2002.

Shen, Q., Wang, H., Shum, C., Jiang, L., Hsu, H. T., and Dong, J.: Recent high-resolution Antarctic ice velocity maps reveal increased mass loss in Wilkes Land, East Antarctica, Scientific reports, 8, 4477, 2018.

Sinninghe Damsté, J. S.: Spatial heterogeneity of sources of branched tetraethers in shelf systems: The geochemistry of tetraethers in the Berau River delta (Kalimantan, Indonesia), Geochimica et Cosmochimica Acta, 186, 13-31, 2016.

Sinninghe Damsté, J. S., Ossebaar, J., Abbas, B., Schouten, S., and Verschuren, D.: Fluxes and distribution of tetraether lipids in an equatorial African lake: constraints on the application of the TEX86 palaeothermometer and BIT index in lacustrine settings, Geochimica et Cosmochimica Acta, 73, 4232-4249, 2009.

Sluijs, A., Pross, J., and Brinkhuis, H.: From greenhouse to icehouse; organic-walled dinoflagellate cysts as paleoenvironmental indicators in the Paleogene, Earth-Science Reviews, 68, 281-315, 2005.

Sluijs, A. and Brinkhuis, H.: A dynamic climate and ecosystem state during the Paleocene–Eocene Thermal Maximum: inferences from dinoflagellate cyst assemblages on the New Jersey shelf, Biogeosciences, 6, 1755-1781, 2009.

Speelman, E. N., Sewall, J. O., Noone, D., Huber, M., von der Heydt, A., Damsté, J. S., and Reichart, G.-J.: Modeling the influence of a reduced equator-to-pole sea surface temperature gradient on the distribution of water isotopes in the Early/Middle Eocene, Earth and Planetary Science Letters, 298, 57-65, 2010.

Stickley, C. E., Brinkhuis, H., Schellenberg, S. a., Sluijs, A., Röhl, U., Fuller, M., Grauert, M., Huber, M., Warnaar, J., and Williams, G. L.: Timing and nature of the deepening of the Tasmanian Gateway, Paleoceanography, 19, 1–18, 2004.

Stocchi, P., Escutia, C., Houben, A. J., Vermeersen, B. L., Bijl, P. K., Brinkhuis, H., DeConto, R. M., Galeotti, S., Passchier, S., and Pollard, D.: Relative sea-level rise around East Antarctica during Oligocene glaciation, Nature Geoscience, 6, 380, 2013.

Taylor, K. W., Huber, M., Hollis, C. J., Hernandez-Sanchez, M. T., and Pancost, R. D.: Re-evaluating modern and Palaeogene GDGT distributions: Implications for SST reconstructions, Global and Planetary Change, 108, 158-174, 2013.

Williams, G., Fensome, R., and MacRae, R.: The Lentin and Williams index of fossil dinoflagellates, 2017 ed, AASP Contrib Ser0160-884348, American Association of Stratigraphic Palynologists Foundation. January, 2017. 2017.

Wilson, D. S., Pollard, D., DeConto, R. M., Jamieson, S. S., and Luyendyk, B. P.: Initiation of the West Antarctic Ice Sheet and estimates of total Antarctic ice volume in the earliest Oligocene, Geophysical Research Letters, 40, 4305-4309, 2013.

Wouters, B., Martin-Español, A., Helm, V., Flament, T., van Wessem, J. M., Ligtenberg, S. R., Van den Broeke, M. R., and Bamber, J. L.: Dynamic thinning of glaciers on the Southern Antarctic Peninsula, Science, 348, 899-903, 2015.

Zachos, J. C., Stott, L. D., and Lohmann, K. C.: Evolution of early Cenozoic marine temperatures, Paleoceanography, 9, 353-387, 1994.

Zachos, J. C., Dickens, G. R., and Zeebe, R. E.: An early Cenozoic perspective on greenhouse warming and carbon-cycle dynamics, Nature, 451, 279-283, 2008.

Zhang, Y. G., Pagani, M., Liu, Z., Bohaty, S. M., and DeConto, R.: A 40-million-year history of atmospheric CO2, Philosophical Transactions of the Royal Society A: Mathematical, Physical and Engineering Sciences, 371, 20130096, 2013.

Zhang, Y. G., Zhang, C. L., Liu, X.-L., Li, L., Hinrichs, K.-U., and Noakes, J. E.: Methane Index: A tetraether archaeal lipid biomarker indicator for detecting the instability of marine gas hydrates, Earth and Planetary Science Letters, 307, 525-534, 2011.

Zhang, Y. G., Pagani, M., and Wang, Z.: Ring Index: A new strategy to evaluate the integrity of TEX86 paleothermometry, Paleoceanography, 31, 220-232, 2016.

Zonneveld, K. A., Versteegh, G. J., Kasten, S., Eglinton, T. I., Emeis, K.-C., Huguet, C., Koch, B. P., de Lange, G. J., de Leeuw, J. W., and Middelburg, J. J.: Selective preservation of organic matter in marine environments; processes and impact on the sedimentary record, Biogeosciences, 7, 2010.

Zonneveld, K. A., Marret, F., Versteegh, G. J., Bogus, K., Bonnet, S., Bouimetarhan, I., Crouch, E., de Vernal, A., Elshanawany, R., and Edwards, L.: Atlas of modern dinoflagellate cyst distribution based on 2405 data points, Review of Palaeobotany and Palynology, 191, 1-197, 2013.

Table captions

Table 1: List of palynomorphs and their abbreviated codes found in the CA-plot (Figure 5). Assumed in situ and reworked dinoflagellate cyst taxa are assigned to Protoperidinioid (P-cyst) taxa and Gonyaulacoid (G-cyst) taxa.

Table 2: Improved age model for the Oligocene of DSDP Site 274 determined by dinocysts biostratigraphy indicators (FO = First occurrence, LO = Last occurrence) and paleomagnetic reversals (chrons).

Figure captions

Figure 1: (a) Ross Sea to Wilkes Land margin bathymetry with present-day locations of DSDP/IODP/CRP drill sites included in this study (red dots). The new data generated for this study comes from DSDP Site 274, marked by yellow dot. The base map is from Quantarctica GIS package, Norwegian Polar Institute. The insert shows the Antarctic continent and the surrounding oceans (divided by gray dotted lines) to give a broader regional context to the study area. (b) A synthesis of paleoceanographic settings at 27 Ma. The paleogeographic position is generated with G-plates (http://www.gplates.org), based on the global plates geodynamic motion model from Müller et al., (2018). Light grey indicates the continental lithosphere. The inferred ocean currents are drawn after reconstructions by Stickley et al., (2004). TC = Tasman current, PLC = Proto-Leeuuwin Current and ACountC = Antarctic Counter Current. Blue arrows indicate cooler ocean currents and red indicate warmer ocean currents. Relative current strength is indicated by arrow size.

Figure 2: (a) Core numbers, core recovery and lithological description of the cores based on the initial DSDP reports (Hayes et al., 1975). (b) Magnetic correlation for Site 274 with comparison to Jovane et al., (2020) (dotted lines). Inclination values define local magnetic polarity zones. Magnetostratigraphic correlation is firstly guided by new dinocyst constraints, biostratigraphic markers from shipboard report and subsequently by correlation between local polarity zones and the GTS2012 timescale (Gradstein et al., 2012). Low intensity, shifting directions, and low recovery precludes magnetozone identification for some intervals. Characteristic orthoplots showing demagnetization steps is included in Supplementary Figure S1. Arrows indicate age (Ma) biostratigraphic tie points according to the age model described in Table 2. Extrapolations has been made between the age tie points (stippled lines) with sedimentation rates indicated in between. LO = Last occurrence, FO = First occurrence.

Figure 3: Correspondence analysis (CA) of the dinocyst assemblage data from DSDP Site 274. The size of the points indicates the total relative abundance of the specific species. The abbreviations of the dinocysts species can be found in Table 1. The data were plotted in the C2 software program (Juggins, 2007). The analysis scores are provided as Table S4.

Figure 4: Lithological (the legend is the same as Figure 2), palynological and TEX_{86}-SST results from DSDP Site 274 plotted against depth. Arrows indicate age (Ma) tie points according to the age model described in Table 2. The dotted gray line indicated the time slices selected for Fig. 5.

(a) The cumulative relative abundance of palynomorph groups.

(b) The cumulative relative abundance (%) of selected dinocysts groups recorded in the studied interval. Blue tones are P-cysts, red-tones are G-cysts.

(c) TEX_{86}-based SSTs (Linear calibration, Kim et al., (2010)), calibration error is ± 5.2°C, indicated by black bar in bottom of the plot. The TEX_{86} outliers are marked in red.

Figure 5: Synthesis of sea surface temperature and dinocysts assemblage changes between the early (c), mid (b) and late Oligocene (a) in the Ross Sea (CRP, DSDP Site 270), offshore Cape Adare (This study, DSDP Site 274) and Wilkes Land margin (Site U1356). The pie charts visualize the dinocyst assemblage composition at respective sites (see legend). Dinocyst assemblage data from the Wilkes Land margin, U1356, comes from Bijl et al., (2018a, b) for all panels (a-c). Dinocyst assemblage data from the Ross Sea is gathered from DSDP Site 270 (Kulhanek et al., 2019) for panel a) and from CRP (Houben et al., 2013; Clowes et al., 2016) for panel (b) and (c). The TEX_{86}-SST data from Wilkes Land, U1356 comes from Hartman et al., (2018), 35 TEX_{86}-data points were used; 7 in (a), 9 in (b) and 19 in (c). In the Ross Sea there is a lack of TEX_{86}-SST data from the mid Oligocene, but Duncan (2017) presented unpublished TEX_{86}-data from CIROS- (12 TEX_{86}-data points), here displayed in panel (c), and from DSDP Site 270, where only one data point matched our mid-early Oligocene time slice in panel (a). All TEX_{86} data have been converted to the SST using linear calibration of Kim et al. (2010) (calibration error: ± 5.2°C). The paleogeographic position is generated with G-plates (http://www.gplates.org), based on the global plates geodynamic motion model from Müller et al., (2018).

Supplementary Information

Supplementary Table S1: Table with a summary of demagnetization data results. Sample identification, Core location indicating core, section and depth (mbsf), Declination, Inclination, Sample intensity (in A/m2), MAD values and remarks including the steps used for interpretation. Resultant orthoplots are depicted in Fig. S1.

Supplementary Table S2: Concentrations of GDGTs at Site 274. All samples and corresponding depths, age of sample, GDGT peak area values, TEX_{86} (Schouten et al., 2002) and BIT index values (Hopmans et al., 2004), Methane Index (Methzhang) values (Zhang et al., 2011), GDGT2/Crenarchaeol ratios (Weijers et al., 2011), GDGT-0/Crenarchaeol ratios (Blaga et al., 2009) and GDGT-2/GDGT-3 ratios (Taylor et al., 2013), and RING index (Sinninghe Damsté, 2016). SST calibrations from Kim et al., 2010; Kim et al., 2012. SSTK10L = linear calibration of Kim et al. (2010). Discarded samples (OUTLIER=TRUE) with outlier values are based on BIT > 0.4, GDGT2/GDGT3` > 5, `GDGT0/cren` > 2 and `Methzhang` > 0.3.

Supplementary Table S3: Total palynomorph assemblage counts DSDP Site 274 cores 43–21.

Supplementary Table S4: Correspondence analysis (CA) scores of the dinocysts assemblage data from DSDP Site 274.

Supplementary Figure S1: Orthogonal plots of representative samples. Most of the samples used for the correlation show two distinctive directions, both in normal samples and in reversed samples. Inclination values are also indicated. Open plots indicate inclinations (vertical projection). All calculated directions are available in Table S1. Samples were calculated by means of the Paldir and paleomagnetism.org (Koymans et al., 2016) programs.

Supplementary Figure S2: Relevant GDGT indices to filter out biased outliers (red crosses) in the generated GDGT data (Table S2), plotted against sample depth (mbsf). The red line marks the limit of reliable values. a) TEX_{86} (Schouten et al., 2002). b) BIT index values (Hopmans et al., 2004). c) Methane Index (Methzhang) values (Zhang et al., 2011). d) AOM index (GDGT2/Crenarchaeol ratios) (Weijers et al., 2011). e) Water column overprint values (GDGT-2/GDGT-3 ratios) (Taylor et al., 2013). f) Methanogenesis values (GDGT-0/Crenarchaeol ratios) (Blaga et al., 2009).

Supplementary Figure S3: Cross plot between the ring index and TEX_{86} values of samples from DSDP Site 274. The lines mark the outer ranges of the ring index (Zhang et al., 2016), outside of which samples have outlying values (marked as crosses). The shade of blue indicates the sample depth (mbsf).

Table 1

***In situ* protoperidioid taxa**	**Code**	***In situ* gonyaulacoid taxa**	**Code**
Brigantedinium pynei	*Br pyn*	*Achomosphaera alcicornu*	*Ac alc*
Brigantedinium simplex	*Br sim*	*Batiacasphaera* spp. pars	*Ba* spp
Brigantedinium spp. pars.	*Br spp*	*Batiacasphaera cooperi*	*Ba coo*
Lejeunecysta spp.pars	*L* spp	*Batiacasphaera compta*	*Ba com*
Lejeunecysta acuminata	*L acu*	*Batiacasphaera* sp. B sensu Bijl et al., 2018	*Ba* spB
Lejeunecysta adeliensis	*L ade*	*Cerebrocysta* spp.	*Cer* spp
Lejeunecysta attenuata	*L att*	*Cleistosphaeridium* sp A. sensu Bijl et al., 2018	*Cl* spA
Lejeunecysta fallax	*L fal*	*Corrudinium* spp. pars	*Co spp*
Lejeunecysta katatonos	*L kat*	*Corrudinium labradori*	*Co lab*
Lejeunecysta rotunda	*L rot*	*Gelatia inflata*	*G inf*
Lejeunecysta sp. A	*L* spA	*Hystrichokolpoma bullatum*	*Hy bul*
Malvinia escutiana	*M esc*	*impagidinium* cf *aculeatum*	*I acu*
Protoperidinium indet.	*Prot*	*Impagidinium cantabrigiense*	*I can*
Selenopemphix antarctica	*Se ant*	*Impagidinium velorum*	*I vel*
Selenopemphix brinkhusii	*Se bri*	*Impagidinium victorium*	*I vic*
Selenopemphix nephroides	*Se nep*	*Impagidinium paradoxum*	*I par*
Selenopemphix spp. pars	*Se* spp	*Impagidinium pallidum*	*I pal*
Dinocyst sp. 1	Dino sp1	*Impagidinium* sp. A sensu Bijl et al., 2018	*I* spA
Reworked peridinioid cysts		*Nematosphaeropsis labyrinthus*	*N lab*
Alterbidinium distinctum	*Al dis*	*Operculodinium* sp. A sensu Bijl et al., 2018	*O spA*
Deflandrea spp. pars	*Df* spp	*Operculodinium centrocarpum*	*O cen*
Moria zachosii	*M zac*	*Operculodinium eirikianum*	*O eir*
Phthanoperidinium spp. pars	*Ph* spp	*Operculodinium janduchenei*	*O jan*
Senegalinium spp.	*Sen* spp	*Operculodinium piasekii*	*O pia*
Spinidinium spp. pars	*Spd* spp	*Operculodinium* spp. pars	*O* spp
Vozzhennikovia spp. pars	*Voz* spp	*Pyxidinopsis* spp.	*Pyx* spp
Other P-cyst reworked	otr-P	*Spiniferites ramous*	*Sf ram*
		Spiniferites bulloideus	*Sf bul*
		Spiniferites spp. pars	*Sf* spp
		Stoveracysta kakanuiensis	*St kak*
		Stoveracysta ornata	*St orn*
		Reworked gonyaulacoid cysts	
		Arachnodinium antarcticum	*A ant*
		Cerebrocysta spp. pars RW	*Cer* RW
		Corrudinium regulare	*Co reg*
		Corrudinium incompositum	*Co inc*
Other palynomorphs		*Enneadocysta* spp. pars	*Enn* spp
Unidentified Dinocyst 1	Indet 1	*Hystrichokolpoma rigaudiae*	*H rig*
Unidentified Dinocyst 2	indet 2	*Hystrichosphaeridium truswelliae*	*Hy tru*
Unidentified Dinocyst 3	indet 3	*Impagidinium* spp. pars RW	*I RW*
Terrestrial	Terr	*Operculodinium* spp. RW	*Ope* RW
Pterospermella/green algae	Ptero	*Pentadinium laticinctum*	*P lat*
Acritarch spp.	Acrit spp	*Thalassiphora pelagica*	*Th pel*
Acritarch chorate/spiney spp.	Acri spiney	*Tuberculodinium vancampoae*	*T van*
Leiosphaeridia	Leios	*Turbiosphaera* spp. pars RW	*Tur* spp
Cymatosphaera spp. pars	Cym Spp	Other G-cyst reworked	otr-G

Table 2

FO/LO	Genus, Chron	Species	Age (Ma)	Depth	Depth error	Event source
	Base of C7n.2n		24.474	199.47		This study
	Base of C9n		27.44	277		This study
	Top of C11n.1n		29.18	321.2		This study
LO	*Stoveracysta*	*ornata*	30.8	323.655	2.015	This study
FO	*Corrudinium*	*labradori*	30.92	362.42	1.24	This study
	Base of C12n		31.03	363.44		This study
FO	*Stoveracysta*	*ornata*	32.5	396.62	5.25	This study
	Base of C13n		33.7	400.17		This study
FO	*Malvinia*	*escutiana*	33.7	404.66	n/a	This study

Figure 1

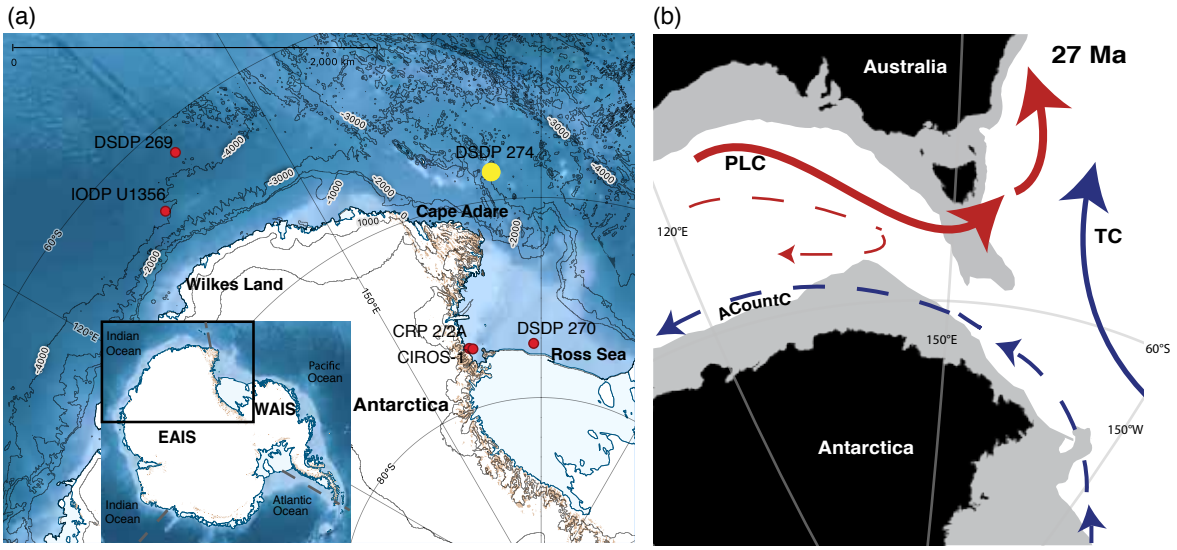
(a)
0
2,000 km
DSDP 269
IODP U1356
DSDP 274
Cape Adare
Wilkes Land
CRP 2/2A
CIROS-1
DSDP 270
Ross Sea
Antarctica
Indian Ocean
Pacific Ocean
WAIS
EAIS
Atlantic Ocean
Indian Ocean
60°S
120°E
150°E
80°S
(b)
Australia
27 Ma
PLC
TC
ACountC
120°E
150°E
60°S
150°W
Antarctica

Figure 2

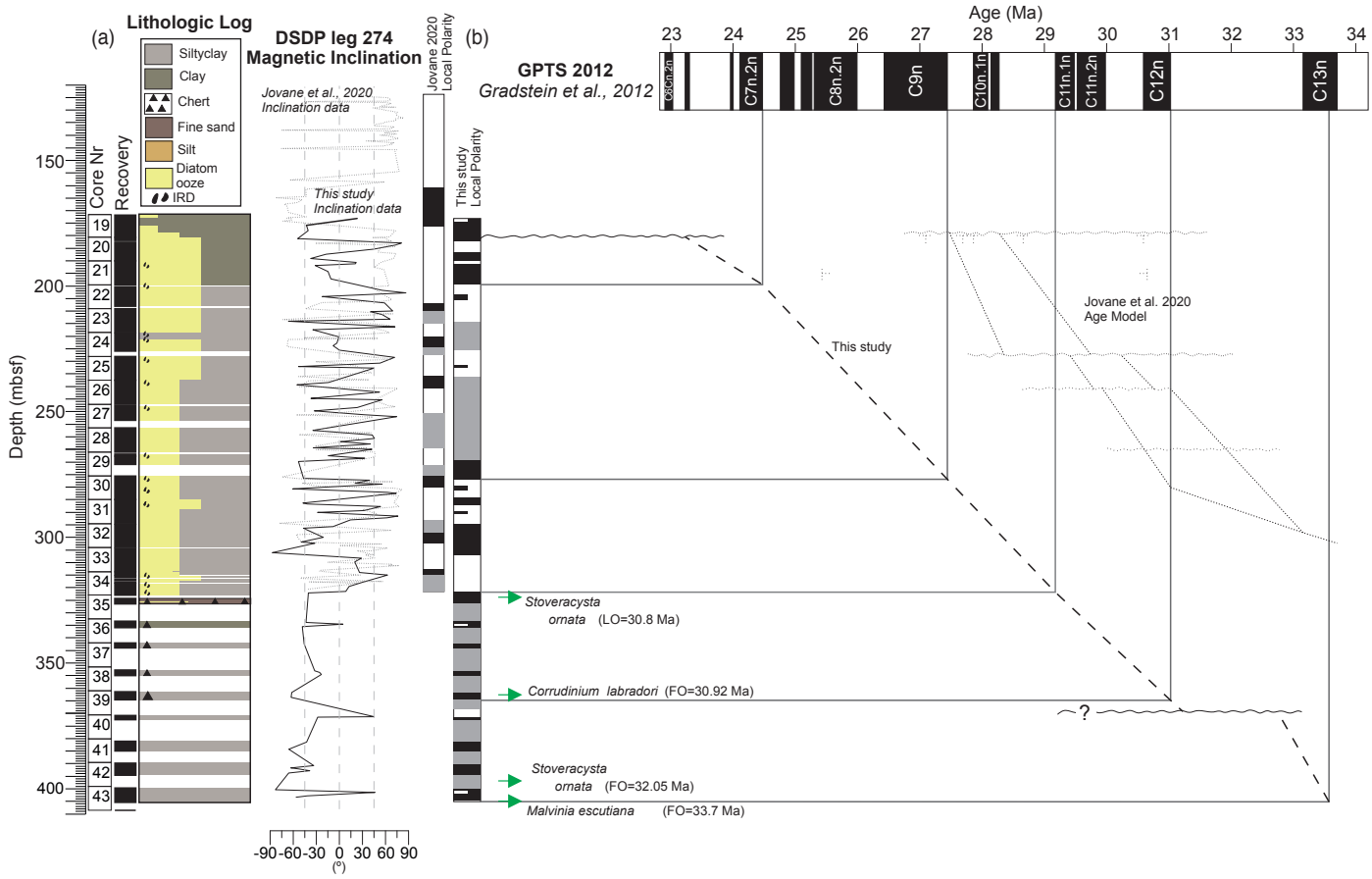
(a)
Lithologic Log
Siltyclay
Clay
Chert
Fine sand
Silt
Diatom ooze
IRD
Core Nr
Recovery
Depth (mbsf)
DSDP leg 274
Magnetic Inclination
Jovane et al., 2020
Inclination data
This study
Inclination data
Jovane 2020
Local Polarity
This study
Local Polarity
-90 -60 -30 0 30 60 90
(°)
(b)
GPTS 2012
Gradstein et al., 2012
Age (Ma)
C7n.2n
C8n.2n
C9n
C10n.1n
C11n.1n
C11n.2n
C12n
C13n
This study
Jovane et al. 2020
Age Model
Stoveracysta ornata (LO=30.8 Ma)
Corrudinium labradori (FO=30.92 Ma)
Stoveracysta ornata (FO=32.05 Ma)
Malvinia escutiana (FO=33.7 Ma)

Figure 3

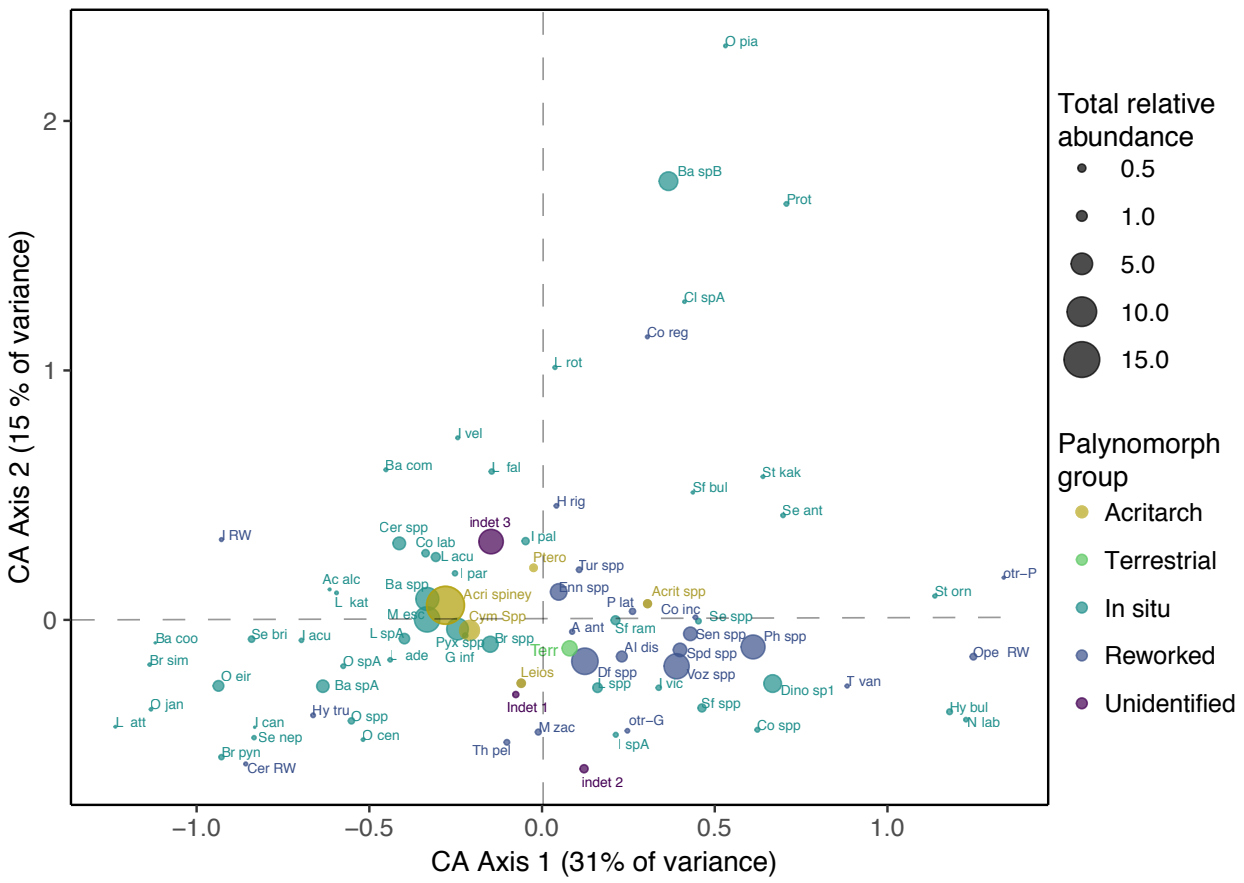
CA Axis 2 (15 % of variance)
CA Axis 1 (31% of variance)
2
1
0
−1.0
−0.5
0.0
0.5
1.0
O pia
Ba spB
Prot
Cl spA
Co reg
L rot
J vel
Ba com
L fal
Sf bul
St kak
H rig
Se ant
J RW
Cer spp
Co lab
indet 3
L acu
I pal
Ptero
Jur spp
Ac alc
I par
Ba spp
Acri spiney
Enn spp
Acrit spp
P lat
Co inc
Se spp
St orn
otr−P
L kat
M esc
Cym Spp
A ant
Sf ram
Sen spp
Ph spp
Ba coo
Se bri
J acu
L spA
Pyx spp
Br spp
Terr
Al dis
Spd spp
Br sim
O spA
L ade
G inf
Df spp
Voz spp
Ope RW
O eir
Ba spA
Leios
L spp
J vic
Dino sp1
J van
O jan
Hy tru
O spp
Indet 1
Sf spp
Hy bul
L att
J can
M zac
otr−G
Co spp
N lab
Se nep
O cen
I spA
Br pyn
Th pel
Cer RW
indet 2
Total relative abundance
0.5
1.0
5.0
10.0
15.0
Palynomorph group
Acritarch
Terrestrial
In situ
Reworked
Unidentified

Figure 4

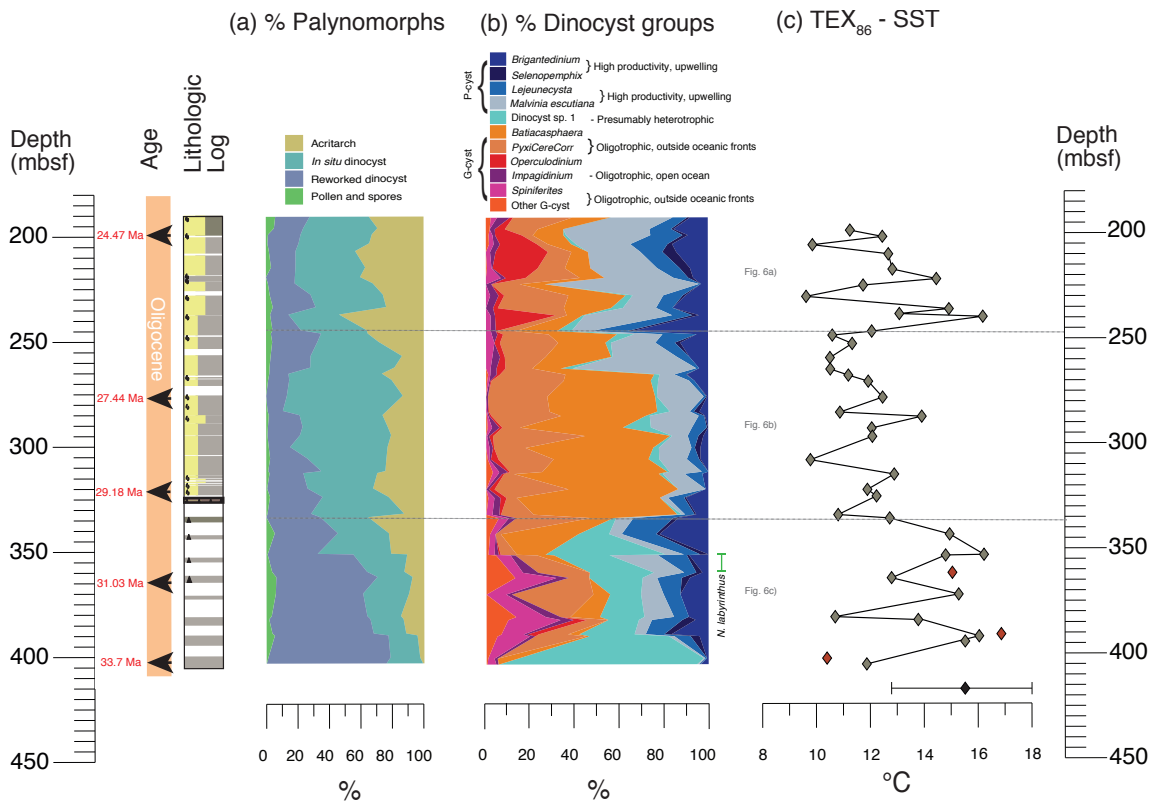
(a) % Palynomorphs
(b) % Dinocyst groups
(c) TEX86 - SST
Depth (mbsf)
Age
Lithologic Log
Oligocene
24.47 Ma
27.44 Ma
29.18 Ma
31.03 Ma
33.7 Ma
Acritarch
In situ dinocyst
Reworked dinocyst
Pollen and spores
P-cyst
Brigantedinium
Selenopemphix
Lejeunecysta
Malvinia escutiana
High productivity, upwelling
Dinocyst sp. 1
Presumably heterotrophic
G-cyst
Batiacasphaera
PyxiCereCorr
Operculodinium
Oligotrophic, outside oceanic fronts
Impagidinium
Oligotrophic, open ocean
Spiniferites
Other G-cyst
Oligotrophic, outside oceanic fronts
N. labyrinthus
Fig. 6a)
Fig. 6b)
Fig. 6c)
%
°C

Figure 5

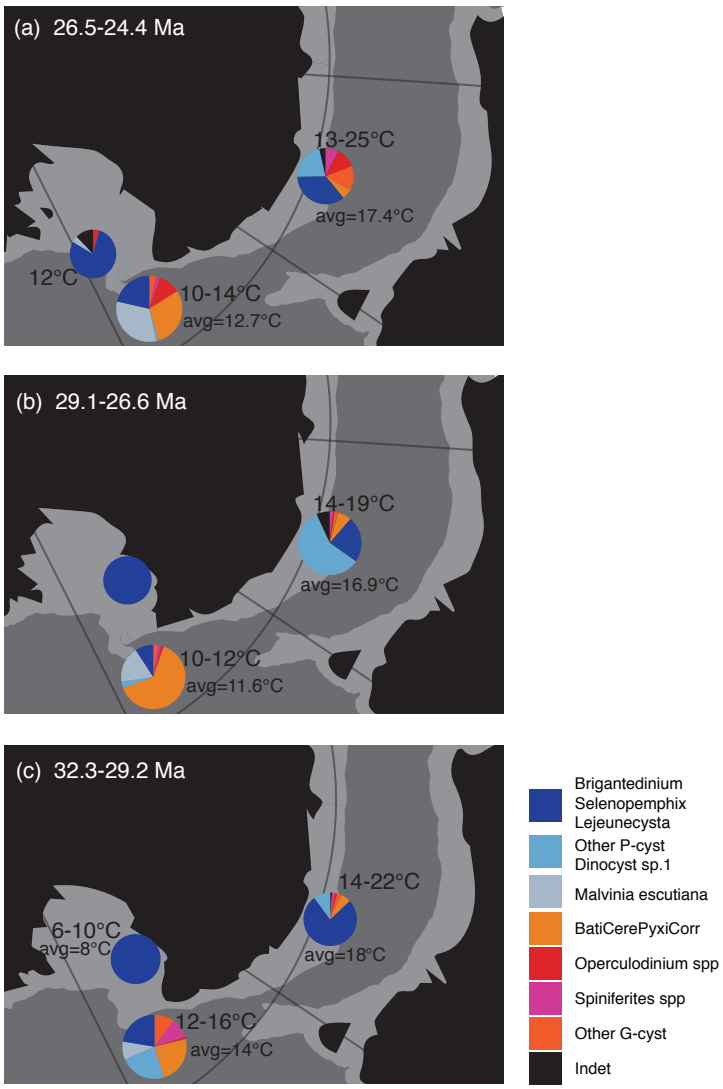
(a) 26.5-24.4 Ma
13-25°C
avg=17.4°C
12°C
10-14°C
avg=12.7°C
(b) 29.1-26.6 Ma
14-19°C
avg=16.9°C
10-12°C
avg=11.6°C
(c) 32.3-29.2 Ma
14-22°C
avg=18°C
6-10°C
avg=8°C
12-16°C
avg=14°C
Brigantedinium
Selenopemphix
Lejeunecysta
Other P-cyst
Dinocyst sp.1
Malvinia escutiana
BatiCerePyxiCorr
Operculodinium spp
Spiniferites spp
Other G-cyst
Indet